The genetic and dietary landscape of the muscle insulin signalling network

Julian van Gerwen[1], Stewart W. C. Masson[1], Harry B. Cutler[1], Alexis Díaz-Vegas[1], Meg Potter[1], Jacqueline Stöckli[1], Søren Madsen[1], Marin E. Nelson[1], Sean J. Humphrey[1], David E. James[1,2,3]

1. Charles Perkins Centre, School of Life and Environmental Sciences, University of Sydney, 2006, Australia

2. Faculty of Medicine and Health, University of Sydney, 2006, Australia

3. Lead contact

Correspondence:

david.james@sydney.edu.au

sean.humphrey@mcri.edu.au

Abstract

Metabolic disease is caused by a combination of genetic and environmental factors, yet few studies have examined how these factors influence signal transduction, a key mediator of metabolism. Using mass spectrometry-based phosphoproteomics, we quantified 23,126 phosphosites in skeletal muscle of five genetically distinct mouse strains in two dietary environments, with and without acute *in vivo* insulin stimulation. Almost half of the insulin-regulated phosphoproteome was modified by genetic background on an ordinary diet, and high-fat high-sugar feeding affected insulin signalling in a strain-dependent manner. Our data revealed coregulated subnetworks within the insulin signalling pathway, expanding our understanding of the pathway's organisation. Furthermore, associating diverse signalling responses with insulin-stimulated glucose uptake uncovered regulators of muscle insulin responsiveness, including the regulatory phosphosite S469 on Pfkfb2, a key activator of glycolysis. Finally, we confirmed the role of glycolysis in modulating insulin action in insulin resistance. Our results underscore the significance of genetics in shaping global signalling responses and their adaptability to environmental changes, emphasizing the utility of studying biological diversity with phosphoproteomics to discover key regulatory mechanisms of complex traits.

Introduction

Protein post-translational modifications such as phosphorylation enable cells to rapidly respond to environmental changes by modifying protein function at low metabolic cost[1]. As a result of this high metabolic efficiency, phosphorylation is involved in nearly all biological processes and is dysregulated in numerous complex diseases[2]. Advances in mass spectrometry-based phosphoproteomics – the unbiased identification and quantification of protein phosphorylation – have led to the discovery of more than 100,000 phosphosites, revealing that the phosphoproteome comprises vast, interconnected phosphorylation networks[3–6], rather than the textbook view of isolated, linear kinase cascades.

The insulin signalling network is among the most studied phosphorylation networks. Post-prandial increases in blood glucose stimulate pancreatic insulin secretion, coordinating a metabolic switch in target tissues like skeletal muscle and adipose[7]. Insulin increases glucose uptake into these tissues by promoting translocation of the glucose transporter GLUT4 to the plasma membrane, and serves other functions like enhancing protein synthesis, downregulating lipid catabolism, and altering gene transcription[7]. To coordinate these functions, insulin triggers a phosphorylation cascade primarily involving activation of the Ser/Thr kinase Akt, regulation of downstream kinases including mTORC1 and GSK3, and modulation of parallel signalling arms[7–9]. Seminal phosphoproteomics studies demonstrated that this cascade regulates over a thousand phosphosites, with many still uncharacterised in insulin action[10–12]. Insulin resistance – the failure of insulin to promote glucose uptake in its target tissues – is triggered by genetic and environmental factors such as family history of metabolic disease and high-calorie diets[13]. Although insulin resistance is a major precursor of metabolic disease including type 2 diabetes, its mechanistic basis remains unresolved[13,14].

Interactions between genetics and environment significantly regulate biomolecular processes, including insulin resistance[15–18]. As signalling pathways connect the extracellular environment to intracellular proteins, they are likely a major conduit of gene-by-environment interactions. Yet, how global phosphorylation signalling networks are regulated across different genetic backgrounds is relatively unexplored. Recent phosphoproteomics studies in yeast[19] and mice[20] identified genetic variants affecting multiple phosphosites, but did not analyse the phosphoproteome's response to acute perturbation, which is crucial to its role as a signal transduction system. We have also shown marked variation in acute signalling responses to exercise or insulin across individuals[21]. However, this study did not systematically assess the relative contributions of genetics and the environment[21]. Understanding how these variables intersect with signal transduction is fundamental to our basic knowledge of signalling and the advancement of personalised medicine, which advocates individualised treatment regimens based on genetic risk factors and gene-by-environment interactions[15,22].

Inbred mice allow precise control of genetics and environment unachievable in human studies, enabling examination of how these factors interact to influence biomolecular systems[23]. Here, we performed phosphoproteomics on insulin-stimulated or control skeletal muscle from five genetically distinct inbred mouse strains fed either an ordinary chow diet or a high-fat, high-sugar "western style"

diet. Strikingly, we found that genetic background influenced both the phosphoproteomic insulin response of chow-fed mice, as well as how these responses were modified by high-fat, high-sugar feeding. These signalling changes were reflected in altered activity profiles of multiple kinases and provided insight into the functional organisation of the insulin signalling network by revealing subnetworks of coregulated phosphosites. A major challenge in phosphoproteomics studies is pinpointing important regulatory events among the many responding to a stimulus. We reasoned that associating changes in protein phosphorylation across the gene-by-environment landscape with phenotypic change – in this case insulin-stimulated glucose uptake – would dissect mechanistic targets with greater fidelity. This approach generated known as well as candidate regulators of insulin-stimulated glucose uptake, leading us to demonstrate that glycolytic upregulation reverses insulin resistance. Our work represents the first global portrait of insulin signalling network plasticity in response to genetic and environmental variation, which will serve as an important resource in future studies of insulin action and resistance.

Results

Phosphoproteomics of insulin signalling in mouse skeletal muscle

To study how protein phosphorylation networks are affected by genetics and environment, we examined insulin signalling in five genetically distinct inbred mouse strains including four lab strains with diverse metabolic phenotypes (C57Bl6J, NOD, BXH9, and BXD34[17]), and the wild-derived CAST strain (**Fig. 1a**). Mice underwent a six-week diet regimen of standard lab diet (CHOW) or a high-fat high-sucrose diet (HFD), which is commonly used to induce insulin resistance[17,24]. Consistent with their diverse genetics, these strains differed in morphometric parameters (body weight, adiposity) and metabolic traits (fasting blood glucose, fasting blood insulin, glucose tolerance) both on the CHOW diet and in their response to HFD-feeding (**Fig. S1**).

We focused on skeletal muscle, as it is the site of greatest post-prandial glucose uptake and the most significant contributor to impaired glucose disposal in type 2 diabetes[25]. Specifically, we chose to examine the soleus muscle, because its largely oxidative fibre composition resembles human muscle tissue more than other murine muscles[26]. Mice were injected retro-orbitally with saline control or insulin for 10 minutes, and the soleus was collected for phosphoproteomic analysis (**Fig. 1a**). A tritiated 2-deoxyglucose (^{3}H-2DG) tracer was co-injected to measure soleus glucose uptake.

Using the EasyPhos workflow and data-independent acquisition (DIA) mass spectrometry[27,28], we quantified 28,809 phosphopeptides across 95 biological samples, corresponding to 23,126 unique high-confidence phosphosites (Class I; localization score > 0.75) on 3,507 proteins (**Fig. 1b, Table S1**). On average we quantified 15,395 phosphopeptides in each sample, with minimal variation (**Fig. S2a**). Samples from animals of the same strain and diet were highly correlated and generally clustered together, implying the data are highly reproducible (**Fig. S2b-d**).

102 To explore the soleus insulin signalling network, we examined phosphopeptides altered by
103 insulin stimulation in at least one of the ten strain-diet combinations. We filtered our data to 10,432
104 phosphopeptides highly quantified across most conditions (see Methods) and identified those with
105 significant differences between unstimulated and insulin-stimulated samples (three-way ANOVA
106 insulin main-effect q-value < 0.05) that was of sufficient magnitude in at least one strain-diet
107 combination (insulin/unstimulated fold change > 1.5). This resulted in 441 insulin-regulated
108 phosphopeptides on 232 proteins, which is noticeably more than recent studies of 10-minute insulin
109 signalling in patient-derived myoblasts (174 phosphopeptides[29] and 242 phosphopeptides[30]) or mouse
110 adipose tissue (319 phosphopeptides[31]) (**Fig. 1b, c, Table S1**).
111 Our analysis recovered many well-studied insulin-regulated phosphosites, including Akt
112 substrates such as T247 on Akt1s1 (PRAS40), S939 on Tsc2, and S9 on Gsk3β (**Fig. 1d-f**), as well as
113 targets of downstream kinases including the Gsk3β substrate S641 on Gys1 (**Fig. 1g**). Enrichment of
114 Gene Ontology (GO) biological processes recapitulated canonical insulin signalling axes including
115 "insulin receptor signaling pathway", "phosphatidylinositol 3-kinase signaling", "protein kinase B
116 signaling", and "TORC1 signaling", and multiple pathways related to glucose metabolism, fatty acid
117 metabolism, autophagy, and protein translation, reflecting known targets of insulin action (**Fig. S3a**).
118 Furthermore, insulin-regulated phosphosites were enriched for insulin regulation in our previous human
119 skeletal muscle phosphoproteome (fold enrichment = 4.22, $p = 9.50 \times 10^{-24}$, one-sided Fisher's exact test,
120 **Fig. S3b**)[21]. Despite this, only half of all insulin-regulated phosphopeptides (228/441) were previously
121 annotated as insulin-regulated in the PhosphositePlus database[32] (**Fig. S3c**), highlighting the potential
122 of our data to discover novel aspects of insulin signalling while recapitulating known components.
123 Overall, our phosphoproteomics data provide a comprehensive and high-quality atlas of insulin
124 signalling in mouse skeletal muscle.
125
126 ***Genetics and diet modulate insulin signalling***
127 The influence of genetic and environmental variation on global insulin signalling responses is largely
128 unknown. We therefore developed a pipeline to address this question using our phosphoproteomics data
129 (**Fig. 2a**). First, we converted the intensity values of each insulin-regulated phosphopeptide to "insulin
130 response" values, by normalising insulin-stimulated data to the unstimulated median of the
131 corresponding Strain-Diet combination. Since protein expression should not change within a 10 min
132 insulin stimulation[31], this allowed us to parse out protein abundance differences across strains and diets
133 and focus solely on acute signalling processes. We then assessed the impact of genetics in CHOW-fed
134 mice by identifying phosphopeptides with differing insulin responses in one or more strains compared
135 to C57Bl6J ("Strain effect"). Lastly, we explored the effects of HFD-feeding on signalling as two types
136 of "Diet effects", either as a "Uniform diet effect" – where HFD-feeding affects each strain similarly –
137 or a "StrainxDiet effect" – where its impact depends on the mouse strain. Analyses of "Strain effects"

138 and "Diet effects" were performed separately, so a phosphopeptide could have both a Strain effect and
139 a StrainxDiet/Uniform Diet effect.

140 Almost half of the 441 insulin-regulated phosphopeptides displayed a Strain effect (**Fig. 2b,**
141 **Table S1**). These included phosphopeptides where C57Bl6J had a stronger insulin response than other
142 strains, such as S15 on the RNA methyltransferase Rnmt (**Fig. 2c**), and phosphopeptides where C57Bl6J
143 had a weaker insulin response, such as S48 on the vesicle fusion regulator Vamp3 (**Fig. 2d**). Vamp3
144 S48 is predicted to be highly functional (functional score = 0.750[33]), its phosphorylation correlates with
145 glucose uptake in insulin-stimulated and/or exercised human skeletal muscle[21], and Vamp3
146 overexpression rescues GLUT4 translocation in insulin resistance[34], suggesting that this site may
147 represent a genetically variable control point of GLUT4 trafficking. In general, insulin responses were
148 weaker in the four remaining strains compared to C57Bl6J, though the extent of this trend was strain-
149 dependent (**Fig. 2e**). In all, the strain-affected phosphopeptides reveal a unique fingerprint of insulin
150 signalling within each strain (**Fig. 2f**), highlighting the complex and widespread effects of genetic
151 variation on signalling networks.

152 We next examined the impact of HFD-feeding in insulin signalling. StrainxDiet effects were
153 more prevalent than Uniform diet effects (110 vs 10 phosphopeptides, **Fig. 2g, Table S1**), suggesting
154 that the molecular impact of dietary perturbation was strongly modulated by genetic background.
155 StrainxDiet effects impacted known regulatory phosphosites such as the inhibitory site S78 on Map2k4,
156 whose insulin response was attenuated by HFD-feeding only in C57Bl6J and CAST (**Fig. 2h**). Map2k4
157 activates p38 and JNK kinases which have been implicated as drivers of HFD-induced insulin
158 resistance[8], and based on the behaviour of S78, the orchestration of this detrimental signalling axis in
159 HFD-feeding may depend on genetic background.

160 HFD-feeding exerted complex effects on signalling, with the balance between suppressed and
161 enhanced insulin responses varying across strains (**Fig. 2i**). Furthermore, insulin-regulated
162 phosphopeptides were largely altered by HFD-feeding in only a single strain, and when multiple strains
163 were affected, they often changed in opposite directions (**Fig. 2j-k**). For instance, multiple insulin
164 responses were strengthened in BXH9 but weakened in C57Bl6J or CAST (**Fig. 2k**), such as S500 on
165 the translation regulator Larp4b (**Fig. S3d)**. Principal component analysis supported the highly
166 divergent impact of dietary perturbation, as HFD-feeding displaced each strain in a distinct direction in
167 principal component space (**Fig. 2l**). StrainxDiet and Strain effects were driven by a mixture of changes
168 to insulin-stimulated phosphorylation, unstimulated phosphorylation, or both, highlighting the
169 complexity of these signalling alterations (**Fig. S3e-f**). This analysis demonstrates the pervasive role of
170 genetics in shaping signalling networks, as genetic background profoundly modulated the effect of
171 HFD-feeding on insulin signalling.
172
173

174 ***Exploring genetic and dietary modulation of the insulin signalling network***

175 To understand the insulin signalling circuitry and functional pathways modulated by genetics and diet,
176 we curated a network of 160 insulin-regulated phosphosites, comprising sites from a knowledge
177 pathway-derived list of canonical insulin signalling proteins[21] and substrates of insulin-regulated
178 kinases (**Fig. 3**, see Methods). Strain and diet affected multiple highly studied signalling sites, including
179 Tsc2 S939 (Diet effect), Gsk3α S21 (Strain and Diet effects), and Tbc1d4 T649 (Strain and Diet effects),
180 while other sites such as Gsk3β S9 and Akt1s1 T247 were unaffected. Interestingly, strain and diet
181 affected both canonical and non-canonical insulin signalling proteins to a similar extent (**Fig. S3g-h**).
182 Non-canonical phosphosites could shed light on underappreciated outcomes of insulin action either
183 altered or unaffected by genetics and the environment, such as the p70S6K substrate S47 on Dnajc2
184 (Strain and Diet effects), which drives cellular senescence[35], and S315 on Pcyt1a (no Strain or Diet
185 effect), which inhibits phosphatidylcholine biosynthesis[36] (**Fig. 3**).

186 No functional pathways were overrepresented within strain or diet-affected phosphosites
187 relative to all insulin-regulated sites, implying that genetics and environment modulate most or all
188 outcomes of insulin. For instance, strain and diet affected regulatory phosphosites controlling vesicle
189 trafficking (S348, T575, S595, and T649 on the GLUT4 trafficking regulator Tbc1d4); glucose
190 metabolism (S469 and S486 on Pfkfb2, which promote glycolysis); mitochondrial structure and
191 function (S129 on Mff, which promotes mitochondrial fission); autophagy (S555 on the master
192 autophagy regulator Ulk1); gene transcription (the inhibitory site S108 on the transcription factor Tfeb);
193 and mRNA translation (S236 on ribosomal proteins S6, S422 on Eif4b, and S64 and T69 on Eif4ebp1,
194 which promote translation). Interestingly, Strain and Diet effects overlapped significantly (fold
195 enrichment = 1.50, $p = 4.40 \times 10^{-9}$, two-sided Fisher's exact test, **Fig. S3i**), implying some phosphosites
196 may be more amenable to regulation overall. As a notable exception, all six insulin-regulated
197 phosphosites on Plin1 had Diet effects while only one had a Strain effect (**Fig. 3**). Plin1 coats and
198 regulates lipid droplets, hence this enrichment of Diet effects may represent a signalling response to
199 increased intramuscular lipids in the HFD condition. Overall, genetics and environment triggered
200 widespread alterations in insulin signalling impinging on diverse cellular pathways.

201

202 ***Genetics and diet rewire insulin-regulated kinase signalling***

203 The extensive signalling changes caused by genetics and diet may result from altered kinase regulation.
204 We tested this hypothesis using a kinase substrate enrichment analysis (KSEA)[37] on phosphopeptide
205 insulin responses. KSEA accurately captured the activation of canonical insulin-regulated kinases (Akt,
206 mTOR, p70S6K, and p90RSK) and the deactivation of GSK3, confirming the validity of the approach
207 (**Fig. 4a**). Focussing on CHOW-fed mice, we identified seven kinases differentially enriched across
208 mouse strains (ANOVA adjusted p-value < 0.05, **Fig. 4b**). For example, insulin activated SGK and
209 deactivated GSK3 more in C57Bl6J and NOD than in other strains (**Fig. 4b**). Extending this analysis to
210 all mice, we identified kinases with Uniform diet or StrainxDiet effects (**Fig. 4c**). Akin to our analysis

211 of individual phosphosites (**Fig. 2**), StrainxDiet effects were more prevalent than Uniform diet effects
212 (five kinases compared to one), indicating that genetic background strongly influences the impact of
213 HFD-feeding on kinase signalling. These results suggest that the observed phosphosite signalling
214 changes could be partly due to altered insulin regulation of multiple kinases.
215
216 ***Biological variation reveals functional organisation of the insulin signalling network***
217 KSEA predicted changes in overall kinase activity, but we questioned if substrates of the same kinase
218 could be differentially regulated by genetic and environmental variation. As a case study we examined
219 substrates of Akt – a master regulator of insulin signal transduction – to assess the similarity of their
220 insulin responses across strains and diets. Strikingly, we observed a range of both positive and negative
221 correlations (**Fig. 5a**). For instance, while Tsc2 S939 and Akt1s1 T247 both activate mTORC1, their
222 insulin responses correlated poorly ($r = 0.202$, $p = 0.168$, **Fig. 5b**). Supporting these findings, similar
223 heterogeneity in Akt substrate insulin responses has previously been observed in skeletal muscle from
224 humans with differing metabolic health[38]. Hierarchical clustering revealed four distinct groups of
225 positively correlated Akt substrates (**Fig. 5a**), suggesting these groups may coordinate distinct
226 functional outputs of Akt signalling.
227 We next explored if the genetic and environmental variation in our study could reveal
228 organisational principles of the entire insulin signalling pathway. By performing weighted gene
229 correlation network analysis (WGCNA[39,40]), we identified eight subnetworks of coregulated insulin-
230 responsive phosphopeptides (**Fig. 5c**) varying in size from 16 to 120 phosphopeptides, with 91 assigned
231 to no subnetwork (**Fig. 5d, Table S2**). Examining the subnetwork "eigenpeptides" – a weighted average
232 of the constituent phosphopeptides[39,40] – revealed that the subnetworks captured distinct effects of
233 genetics and diet on insulin signalling (**Fig. 5e**). For example, HFD-feeding attenuated the insulin
234 response of subnetwork I in CAST and C57Bl6J strains, while subnetwork II was affected by HFD-
235 feeding only in CAST and NOD (**Fig. 5e**). This suggests that the subnetworks may be sensitive to
236 distinct cellular information.
237 Next, we characterised the regulatory and functional nature of these subnetworks. Canonical
238 insulin-regulated kinases such as Akt and mTOR were enriched across multiple subnetworks (**Fig. 5f**),
239 confirming that genetic and environmental variation can reveal uncoupling of substrates targeted by the
240 same kinase (**Fig. 5a-b**). Nevertheless, visualising these subnetworks within our curated insulin
241 signalling pathway (**Fig. 3**) revealed cases where signal flowed through a single subnetwork, such as
242 from Erk2 (Y185) to its target kinase Rsk2 (T365 and S369) and Rsk2 substrates (Gab2 S211 and Nos1
243 S847) within subnetwork III (**Fig. S4**). Within multiply phosphorylated proteins, phosphosites either
244 belonged to the same subnetwork (e.g. Plin1) or diverse subnetworks (e.g. Tbc1d4 and the transcription
245 factor Nfatc2), suggesting the latter may serve as hubs integrating diverse cellular information (**Fig. S4**).
246 Some subnetworks were enriched in specific cellular compartments (GO ontologies), implying
247 that common localisation may facilitate coregulation of phosphosites (**Fig. 5g**). Coregulation may

248 partition functional outcomes of insulin action, as certain biological processes were enriched only in
249 select subnetworks (**Fig. 5h**). These included known insulin targets like "negative regulation of lipid
250 catabolic process" in subnetwork I and "positive regulation of glycogen biosynthetic process" in I, VI,
251 and VIII (**Fig. 5h**). Lastly, we leveraged our previous phosphoproteomic time course of insulin
252 signalling to interrogate subnetwork dynamics[10] and found that phosphopeptide insulin response
253 dynamics varied across subnetworks (**Fig. 5i**). This reveals distinct temporal regulation as another
254 feature underlying the substructure of the insulin signalling network. Overall, genetic and
255 environmental diversity illuminated the complex coregulation structure of insulin signalling, featuring
256 subnetworks that evade known network circuitry and present unique functional signatures.
257
258 ***Leveraging biological variation to identify drivers of insulin responsiveness***
259 We have so far described the marked influence of genetic background and HFD-feeding on skeletal
260 muscle insulin signalling, evident at the level of individual phosphosites, protein kinases, and co-
261 regulated network modules. We hypothesised that by associating this signalling diversity with a
262 phenotypic output of insulin, such as enhanced glucose uptake, we would filter out mechanistically
263 irrelevant phosphosites and hence prioritise molecular regulators of the phenotype. To test this
264 hypothesis, we measured *in vivo* glucose uptake with ^{3}H-2DG tracer in the same muscle samples used
265 for phosphoproteomics. Insulin-stimulated glucose uptake differed by more than twofold across strains
266 (two-way ANOVA strain effect $p = 4.78 \times 10^{-7}$) and was almost uniformly decreased by HFD-feeding
267 (two-way ANOVA diet effect $p = 1.83 \times 10^{-5}$) (**Fig. 6a**). This highlights that genetic background and
268 dietary status are key determinants of insulin responsiveness.
269 To prioritise signalling nodes responsible for differences in insulin responsiveness, we correlated
270 all insulin-regulated phosphopeptides with glucose uptake in insulin-stimulated muscles, resulting in
271 37 significantly correlated phosphopeptides ($r > 0.35$ or < -0.35, q-value < 0.1, **Fig. 6b**). The most
272 significantly correlated phosphopeptide contained T1174 and S1176 on the nitric oxide synthase Nos3.
273 The latter serves as a positive control for our analysis, as this site is known to be phosphorylated in
274 response to insulin to promote *in vivo* glucose uptake by vasodilation[41–43] (**Fig. 6c**). Other correlated
275 phosphopeptides that could modulate insulin responsiveness include S1751 on Afdn, a phosphosite
276 implicated in insulin action[44], and S196 on the Prkag2 subunit of AMPK, a major metabolic signalling
277 hub promoting glucose uptake[45] (**Fig. 6b**). These examples suggest that our analysis prioritised
278 regulators of glucose uptake.
279 While the above analysis identified phosphosites associated with glucose uptake through their
280 absolute abundance, we hypothesized that for some phosphosites, the magnitude of their response to
281 insulin may be a stronger determinant of insulin action. We found that the insulin response values of 13
282 phosphopeptides correlated with insulin-stimulated glucose uptake ($r > 0.35$ or < -0.35, q-value < 0.1,
283 **Fig. 6d**). These were largely distinct from the 37 phosphopeptides identified in our first analysis,
284 indicating that the two approaches captured complementary information. Several of these

285 phosphopeptides could regulate insulin-stimulated glucose uptake, such as the regulatory site S469 on
286 the enzyme Pfkfb2 which activates glycolysis, a major pathway for glucose consumption[46–48] (**Fig. 6e**),
287 and S177 on Rcsd1, which could affect GLUT4 vesicle transport via actin cytoskeleton remodelling[49]
288 (**Fig. 6d**).
289 In addition to individual phosphosites, the status of larger signalling network components could
290 also influence insulin responsiveness. Kinase enrichment scores affected by strain or diet did not
291 correlate with glucose uptake (**Table S3**), suggesting insulin action is not dominated by the net activity
292 of specific kinases. Interestingly, two WGCNA-derived insulin signalling subnetworks correlated with
293 glucose uptake: subnetwork V ($r = 0.436$, $p = 0.00173$) and subnetwork I ($r = 0.332$, $p = 0.0197$, **Fig.**
294 **6f**). Subnetwork V could modulate glucose uptake through actin cytoskeleton remodelling via Rscd1
295 S177, through glucose metabolism promotion via Gys1 S641 (**Table S2**), and by influencing GLUT4
296 vesicle trafficking due to its enrichment at "cytoplasmic vesicle membranes" (**Fig. 5g**). It was also
297 enriched in substrates of GSK3, which has been implicated in insulin resistance in skeletal muscle[50–52]
298 and adipose tissue[31]. Subnetwork I, the largest cluster containing 27% of insulin-regulated
299 phosphopeptides, was enriched in multiple kinases and biological processes (**Fig. 5f, h**), suggesting it
300 may be a central regulatory hub for various outcomes of insulin action including glucose uptake. Overall,
301 compartmentalisation of insulin-responsive phosphosites into subnetworks may enable independent
302 control of insulin's functional outputs, since only two subnetworks correlated with insulin-stimulated
303 glucose uptake.
304
305 ***Upregulating glycolysis reverses insulin resistance***
306 We next aimed to validate our approach for identifying regulatory mechanisms of insulin-stimulated
307 glucose uptake. S469 on Pfkfb2 correlated highly with glucose uptake follow insulin stimulation (**Fig.**
308 **6e**). Phosphorylation of this site leads to increased production of F2,6BP, a potent glycolytic agonist,
309 suggesting that activating glycolysis may play a key role in muscle insulin responsiveness. This is
310 consistent with our previous findings that glycolytic enzyme abundance was strongly associated with
311 *ex vivo* insulin-stimulated glucose uptake in muscle from inbred mice[17], and that decreasing glycolytic
312 flux caused insulin resistance *in vitro*[53]. To further establish glycolysis as a regulator of insulin
313 responsiveness in skeletal muscle, we decided to investigate whether upregulating glycolysis through
314 F2,6BP production can restore insulin-stimulated glucose uptake in insulin resistance. We endeavoured
315 to stimulate glycolytic flux in muscle cells independently of regulatory input in case this is compromised
316 by insulin resistance. While Pfkfb2 requires activating phosphorylation by Akt to produce F2,6BP
317 substantially, its paralog Pfkfb3 has high basal production rates and lacks an Akt motif at the
318 corresponding phosphosites[48]. We therefore rationalised that overexpressing Pfkfb3 would robustly
319 increase F2,6BP production and enhance glycolysis regardless of insulin stimulation and Akt signalling
320 (**Fig. 6g**). To avoid systemic effects of Pfkfb3 overexpression we studied cultured L6-GLUT4-HA

321 myotubes, which display robust insulin regulation of GLUT4 trafficking and develop insulin resistance
322 upon palmitate treatment, mimicking lipotoxicity, a trigger of *in vivo* insulin resistance[54].
323 As anticipated, Pfkfb3 overexpression increased glycolytic capacity in L6-GLUT4-HA myotubes
324 as measured by extracellular acidification rate (**Fig. S5a-c**). Pfkfb3 overexpression also restored insulin-
325 stimulated glucose uptake to normal levels in palmitate-treated cells (**Fig. 6h**). This effect was only
326 observed in cells treated with palmitate and insulin, suggesting it specifically modulated insulin action
327 rather than non-specifically increasing glucose uptake through enhanced glucose consumption. These
328 results further establish glycolytic flux as a major determinant of the glucose uptake arm of muscle
329 insulin action and highlight the power of studying phosphoproteomics across the gene-by-environment
330 landscape to identify causal drivers of complex phenotypes. We anticipate that our catalogue of glucose
331 uptake-correlated phosphosites will provide a rich starting point for future investigations into
332 mechanisms of insulin action and resistance.

Discussion

The environment shapes the flow of information from genotype to phenotype. Many studies have interrogated the role of intermediate molecular layers such as the transcriptome or proteome, however few studies have examined how protein post-translation modifications participate in this information transfer. Here we have approached this problem by leveraging diverse inbred mouse strains and phosphoproteomics to examine the insulin signalling network across a landscape of genetic and dietary variation. Genetic background significantly altered the insulin signalling network both independently and in concert with dietary status, affecting myriad phosphosites and multiple kinases. We exploited this variation in signalling responses in two ways – to study the partitioning of the Akt and insulin signalling pathways into distinct subnetworks of coregulated phosphosites; and to identify potential regulators of insulin responsiveness by associating phosphorylation with insulin-stimulated glucose uptake. Finally, validation studies in L6 myotubes confirmed the major role of accelerated glycolysis as a key regulator of insulin responsiveness.

Genetic and diet-driven signalling changes did not transmit linearly through our current model of the insulin signalling network, illustrating that this model remains incomplete. Notably, substrates of kinases such as Akt clustered into distinct groups based on differing insulin responses. Hence, it is an oversimplification to model signalling pathways as networks of individual kinases since substrates of the same kinase display independent regulation. This could arise from localisation of a kinase to distinct substrate pools[55–57]; interactors targeting a kinase to different substrates[55]; substrate phosphorylation by alternate kinases[58]; the dephosphorylation of specific substrates by phosphatases; kinase post-translational modifications altering substrate specificity; and distinct substrate phosphorylation kinetics[10]. As our knowledge of the repertoire of kinase substrates continues to deepen[59], future research should explore how the above mechanisms contribute to finer regulation of these substrates. Genetic and environmental variation also exposed a coregulation subnetwork structure within the insulin signalling network. The enrichment of subnetworks in distinct biological processes, and the selective association of two subnetworks with glucose uptake, suggests that this coregulation structure may direct independent control of distinct outcomes of insulin action. This exciting possibility necessitates further investigation, including replication in independent cohorts, spatiotemporal characterisation of subnetwork dynamics, and association of additional insulin-regulated phenotypes with subnetwork profiles.

Muscle insulin signalling responses vary across individuals[21,38], and our results suggest that baseline genetic differences and an individual's environment both alter signalling, with the environment's influence depending strongly on genetic background. Signalling pathways are popular therapeutic targets due to their importance in human health and the relative ease of pharmaceutical interventions[60]. Our results advocate for a personalised approach to such therapies, implying that the efficacy of treatments aiming to correct pathological signalling responses will depend on an individual's genetic background. In cancer, where signalling networks are dysregulated heterogeneously, modelling

370 patient-specific networks has already shown promise for identifying personalised drug targets[61,62].
371 Personalised medicine approaches will also be aided by a comprehensive understanding of how genetics
372 shape signalling networks and potentiate their modulation by the environment. Recent studies have
373 made the first step, revealing that the ground-state phosphoproteome can be altered by mutations
374 affecting network components such as kinases, phosphatases, and phosphoproteins, as well as the
375 molecular milieu the network is exposed to including extracellular signalling ligands[19,20]. An important
376 corollary of such genetic factors is that multiple genetic backgrounds should be studied when
377 establishing generalizable signalling responses. Our data indicate that insulin responses in C57BL6J –
378 the most commonly studied mouse strain – are not necessarily generalizable, indicated by phosphosites
379 such as S15 on Rnmt that were insulin regulated almost exclusively in C57Bl6J.

380 A major challenge in studying signal transduction with omics technologies is that hundreds to
381 thousands of molecular events typically respond to a cellular signal, making it difficult to pinpoint the
382 most crucial regulatory nodes. To tackle this challenge, we previously demonstrated that associating
383 phosphoproteomics with physiological phenotypes across diverse individuals enriches for phosphosites
384 more likely to modulate biological responses[21]. Here we have elaborated on this approach, revealing
385 that associating phosphorylation with phenotype across a genetic and environmental landscape can
386 identify regulators of specific biological processes, such as insulin-stimulated glucose uptake. Our
387 results recapitulated known glucose uptake regulators and led to further validation of glycolytic flux as
388 a modulator of insulin responsiveness. We have previously demonstrated that reduced glycolytic flux
389 impairs GLUT4 translocation and insulin signalling[53], implying that the status of glycolysis is sensed
390 by proteins regulating insulin action. An enhanced glycolytic metabolic tone may alter production of
391 reactive oxygen species, a known modulator of insulin action[54,63,64] and insulin signalling[65].
392 Alternatively, recent approaches to map protein-metabolite interactions could identify points of
393 allosteric crosstalk between glycolytic metabolites and insulin action proteins[66,67], hence broadening our
394 understanding of the bidirectional communication between insulin action and metabolism.

395 It was striking that only several dozen insulin-regulated phosphopeptides associated significantly
396 with glucose uptake. Since insulin triggers multiple distinct cellular outcomes, it is possible that only a
397 subset of insulin-responsive phosphosites contribute to enhanced glucose uptake. Moreover, many of
398 these phosphosites might only be permissive for insulin-stimulated glucose uptake and are not major
399 regulatory nodes determining the fidelity of the process. For example, while mutation of the four
400 primary Akt regulatory sites on Tbc1d4 blocks GLUT4 translocation[68], none of these phosphosites
401 featured strong positive correlations with glucose uptake in our analysis (**Fig. S6**). This implies that
402 their phosphorylation may promote glucose uptake in a functionally permissive, switch-like fashion.
403 We suggest that the glucose uptake-associated phosphosites we have identified will be enriched in major
404 regulators of insulin responsiveness, necessitating future functional studies to characterise these sites
405 and explore their involvement in insulin resistance.

406 Our work demonstrates that genetic and environmental variation can profoundly modulate global
407 signalling networks and that the influences of these factors are intrinsically entwined. We show that the
408 resulting diversity in signalling responses can be leveraged to pinpoint regulators of insulin-stimulated
409 glucose uptake, providing a powerful methodological framework for interrogating the regulatory basis
410 of complex biological pathways.
411

412 ***Limitations of this study***

413 First, this study focused on male mice and examined only five inbred strains. This limited number of
414 strains may mean that our association analysis was underpowered to detect some regulators of insulin
415 responsiveness. Importantly, however, this does not imply that the regulators identified are incorrect,
416 but only that there may be more to discover with larger cohorts. Future work should therefore extend
417 our approach across a broader range of genetic backgrounds, as well as in female mice. Second, we
418 only examined insulin signalling after 10 minutes, since measuring multiple timepoints would have
419 drastically increased the number of animals and samples required. Integration of dynamic
420 phosphoproteome data from cultured cells indicated that insulin signalling dynamics may contribute to
421 trends in our data (**Fig. 5i**), suggesting the exploration of signalling at additional timepoints may be
422 fruitful in the future. Third, mammalian tissues are a heterogeneous mixture of cell types, and
423 differences in this mixture could result in different signalling responses measured at the whole tissue
424 level. In our experience, the soleus can be reproducibly dissected as an intact muscle with little
425 contamination from surrounding tissues, making it unlikely that cell type composition varied across
426 samples due to tissue collection. However, we cannot exclude the possibility that differences in the
427 composition of the soleus muscle across strains and diets contributed to the signalling changes we
428 detected. Lastly, as we did not perform total proteomics in parallel to phosphoproteomics, we did not
429 assess whether phosphosite changes were caused by differences in total protein abundance. While we
430 cannot ignore the influence of changes in protein abundance, in our previous studies of insulin signalling
431 in adipocytes[31] or human skeletal muscle[21] in which deep proteomes were measured in parallel, we
432 found little global correlation between changes in protein phosphorylation and protein abundance in
433 both unstimulated and insulin-stimulated conditions, suggesting the contribution of protein abundance
434 to phosphosite changes is likely minimal.
435

436 **Additional information**

437 ***Acknowledgements***

438 D.E.J. is an Australian Research Council (ARC) Laureate Fellow. The content is solely the
439 responsibility of the authors and does not necessarily represent the official views of the ARC. The
440 authors also acknowledge the facilities, and the scientific and technical assistance of the Sydney Mass
441 Spectrometry Facility and the Laboratory Animal Services at the Charles Perkins Centre, University of
442 Sydney.

443

444 ***Author Contributions***

445 Conceptualization: JvG, SWCM, SJH, DEJ. Methodology: JvG, HBC, SWCM, ADV, MP, SJH. Formal
446 analysis: JvG. Investigation: JvG, SWCM, HBC, ADV, MP, JS, SM, MEN, SJH. Resources: JS.
447 Writing – Original Draft: JvG. Writing – Review and Editing: All authors. Visualization: JvG.
448 Supervision: SWCM, SJH, DEJ. Project Administration: JvG, SWCM, SJH, DEJ. Funding Acquisition:
449 DEJ

450

451 ***Declaration of Interests***

452 The authors declare no competing interests.

453

454 ***Data Access Statement***

455 All raw and Spectronaut processed phosphoproteomics data have been deposited in the PRIDE
456 proteomeXchange repository and will be made publicly available upon publication. Processed data are
457 available as supplementary tables.

458

459 ***Code availability***

460 All code used to analyse data and produce figures has been uploaded to
461 https://github.com/JulianvanGerwen/GxE_muscle_phos

462

463 **Methods**

464 ***Statistical analysis***

465 Most statistical analysis was performed in the R programming environment using RStudio (R version:
466 4.2.1, RStudio version: 2022.07.1 Build 554). Analysis of GLUT4-HA-L6 myotube Pfkfb3 expression,
467 2DG uptake, and ECAR was performed in GraphPad Prism (version: 9.3.1).

468

469 ***Animal details***

470 Male C57BL/6J (C57Bl6J), BXH9/TyJ (BXH9), BXD34/TyJ (BXD34), and CAST/EiJ (CAST) mice
471 were purchased from Australian BioResources (Moss Vale, NSW, Australia) while NOD/ShiLtJ (NOD)
472 mice were purchased from Animal Resources Centre (Murdoch, WA, Australia). Mice were at most 9
473 weeks old upon arrival. Mice were housed at 23 °C on a 12 h light/dark cycle in cages of 2-5, with free
474 access to food and water. At 12-16 weeks of age mice were randomly allocated to a standard CHOW
475 diet (13% calories from fat, 65% from carbohydrate, 22% from protein; "Irradiated Rat and Mouse
476 Diet", Specialty Feeds, Glen Forrest, WA, Australia) or a high-fat high-sucrose diet made in house
477 (HFD; 45% calories from fat (40% calories from lard), 35% from carbohydrate (14% calories from
478 starch), and 22% from protein) and sacrificed exactly 6 weeks later. The number of mice in each group
479 are C57Bl6J: 8 CHOW, 10 HFD; NOD: 10 CHOW, 10 HFD; BXH9: 8 CHOW, 9 HFD; CAST: 9

480 CHOW, 9 HFD; BXD34: 10 CHOW, 11 HFD. Procedures were carried out with approval from the
481 University of Sydney Animal Ethics Committee following guidelines issued by NHMRC (Australia).
482
483 ***Assessment of body composition***
484 Body composition of individual mice was assessed using the EchoMRI-900 to determine lean mass 1
485 day before a glucose tolerance test and 5-6 days before euthanasia. Analysis was performed as per the
486 manufacturer's specifications.
487
488 ***Glucose tolerance test***
489 On the day of a glucose tolerance test mice were fasted for 6 h (0800-1400). Mice were then orally
490 gavaged with 20% (w/v) glucose in water at 2 g/kg lean mass, and blood glucose was measured from
491 the tail vein using a glucometer 0, 15, 30, 45, 60, and 90 min after the gavage. At 0 and 15 min, 5 µL
492 blood was also collected into an Insulin Mouse Ultra-Sensitive ELISA plate (Crystal Chem USA, Elk
493 Grove Village, Illinois, USA). Blood insulin concentration was measured according to the
494 manufacturer's protocol, using linear extrapolation from an insulin standard curve. The area of the blood
495 glucose curve (AOC) was calculated by:

496 $$\mathrm{AOC} = \sum_{i=2}^{n} \frac{(G_{i-1} - G_1) + (G_i - G_1)}{2}(t_i - t_{i-1})$$

497 Where i represents the ith timepoint at which blood glucose was measured, n represents the last
498 timepoint, t_i represents the time (min) of the ith timepoint, and G_i represents blood glucose
499 concentration (mM) at the ith timepoint.
500
501 ***In vivo insulin stimulation***
502 On the day of the procedure mice were fasted for 2h (1100-1300). Mice were then anaesthetised by
503 intraperitoneal injection of sodium pentobarbital at 80 mg/kg body mass. To counter anaesthesia-
504 associated declines in body temperature, mice were wrapped in aluminium foil and placed on a heating
505 pad at 37°C. After 15 min anaesthesia, mice were injected retro-orbitally as previously described[69] with
506 50 µL plasma replacement (B. Braun, Melsungen, DEU) containing 10 µCi ^{3}H-2DG and saline or
507 insulin (0.75 U/kg lean mass). Blood glucose was measured from the tail vein using a glucometer
508 (AccuCheck, Roche Diabetes Care, NSW, Australia) 1 min prior to injection and 1, 5, 7.5, and 10 min
509 after injection. Simultaneously, 5 µL blood was collected into 95 µL 0.9% NaCl on ice to measure ^{3}H-
510 2DG blood concentration. Ten minutes after insulin injection mice were sacrificed by cervical
511 dislocation and the soleus muscle was rapidly excised, immediately frozen in liquid nitrogen, and stored
512 at -80°C. To measure ^{3}H-2DG blood concentration, diluted blood samples were first centrifuged at
513 10,000 xg for 10 min to pellet blood cells. Supernatant (70 µL) was collected and combined with 3 mL
514 liquid scintillation cocktail (Perkin Elmer, Massachusetts, USA: 6013321) to allow the measurement of
515 ^{3}H with a Tri-Carb 2810TR Liquid Scintillation Counter (Perkin Elmer, Massachusetts, USA).

516

517 ***Skeletal muscle lysis***

518 Frozen muscle tissue was powdered by grinding in a mortar and pestle chilled with liquid nitrogen and
519 dry ice. To lyse powdered tissue, 200 µL lysis buffer (4% (w/v) sodium deoxycholate, 100 mM Tris-
520 HCl pH 8.5) was added followed by 10 s vortexing. Samples were then sonicated at 4 °C at 90% power
521 using pulses of 2 s on, 5 s off for a total time of 1 min. Samples were then immediately boiled at 95 °C
522 with 1,500 rpm shaking for 5 min and sonicated for a further 2 min (4 °C, 90% power, 5 s on and 5 s
523 off) to ensure complete lysis. Lysate was then centrifuged at 20,000 xg for 5 min and 180 µL supernatant
524 was collected. Cysteine residues were reduced and alkylated by adding 40 mM chloroacetamide and 10
525 mM TCEP at pH 7. Lysate was incubated for 5 min at 45 °C with 1,500 rpm shaking and then incubated
526 for a further 40 min at room temperature without shaking.

527 Next, 800 µL 100% chloroform and 1,600 µL 100% methanol were added following 30 s
528 sonication at 90% power. LC/MS grade water (800 µL) was added following 5 min mixing at 1,000
529 rpm. Lysate was centrifuged for 5 min at 2,000 xg to induce a phase separation. The majority of the
530 aqueous phase (2,400 µL) was removed and 2,000 µL was reserved for ^{3}H-2DG quantification. Next,
531 2,400 µL 100% methanol was added following 30 s mixing at 800 rpm and centrifugation at 2,000 xg
532 for 5 min. The supernatant was discarded, and the protein pellet was air-dried for 5 min. Protein was
533 reconstituted in 200 µL lysis buffer, sonicated at 60% power for 15 s using a tip-probe sonicator and
534 boiled for 5 min in a thermomixer at 95 °C with 1,500 rpm shaking.

535

536 ***Determining ^{3}H-2DG uptake into muscle tissue***

537 Anion exchange chromatography was used to quantify ^{3}H-p2DG, representing ^{3}H-2DG that has been
538 taken up by cells. For quantification of total (phosphorylated and unphosphorylated) ^{3}H-2DG, 375 µL
539 lysate aqueous phase was combined with 1,125 µL water and reserved. For quantification of
540 unphosphorylated ^{3}H-2DG, 1,000 µL lysate aqueous phase was added to 300 µL 37.5% (w/v) AG 1-
541 X8 anion exchange resin (Bio-Rad, Hercules, CA, USA: 1401441) and washed with 3 mL water to
542 remove p2DG. Liquid scintillation cocktail (3 mL) was then added to 1,500 µL total and
543 unphosphorylated ^{3}H-2DG solutions, and ^{3}H-2DG was measured using a Tri-Carb 2810R Liquid
544 Scintillation Counter. Unphosphorylated and total ^{3}H-2DG scintillation counts were subtracted to
545 quantify ^{3}H-p2DG.

546 ^{3}H-2DG blood concentration at 1, 5, 7.5, and 10 min after injection was fit to an exponential
547 curve $y = C_p(0)e^{-K_p t}$ where $C_p(0)$ represents the predicted initial tracer concentration (DPM/µL) and
548 K_p represents the rate of tracer disappearance from the blood (1/min), to model the disappearance of
549 ^{3}H-2DG from the blood as it is taken up and trapped by peripheral tissues[70]. $C_p(1)$ was removed when
550 it was abnormally low ($C_p(1) < C_p(5),\ C_p(5) - C_p(1) > 0.5 \times (C_p(5) - C_p(7.5))$), which likely
551 indicates insufficient diffusion of circulating ^{3}H-2DG into the tail vein. To account for different rates
552 of blood ^{3}H-2DG disappearance across mice, ^{3}H-2DG uptake was calculated as a rate constant[70]:

553 $$K_i = \frac{C_i(t)K_p}{C_p(0)(1 - e^{-K_p t})}$$

554 Where t represents the time after injection that the animal was sacrificed (min) and $C_i(t)$ represents the
555 concentration of ^{3}H-p2DG in the tissue harvested at time t (DPM/mg tissue).
556
557 ***Phosphoproteomics sample preparation***
558 Phosphopeptides were isolated using the EasyPhos protocol[27] with minor modifications. Protein
559 (C57Bl6J and NOD: 755 µg, BXH9 and BXD34: 511 µg, CAST: 364 µg) was digested into peptides
560 by incubation in 1% (w/w) Trypsin and LysC on a thermomixer at 37°C with 1,500 rpm shaking for 14
561 h. Following digestion, 400 µL 100% isopropanol and 100 µL EasyPhos enrichment buffer (48% (v/v)
562 TFA, 8 mM KH_2PO_4) were sequentially added with mixing (1,500 rpm, 30 s) after each addition. Lysate
563 was centrifuged at 20,000 xg for 15 min to pellet insoluble material and transferred to a deep well plate.
564 The EasyPhos protocol was then followed from step 12[27].
565
566 ***Liquid chromatography-tandem mass spectrometry (LC-MS/MS)***
567 Enriched phosphopeptides in MS loading buffer (2% ACN, 0.3% TFA) were loaded onto in-house
568 fabricated 55 cm columns (75 µM I.D.), packed with 1.9 µM C18 ReproSil Pur AQ particles (Dr.
569 Maisch HPLC GmbH, Ammerbuch, DEU) with a Dionex U3000 HPLC (Thermo Fisher Scientific),
570 interfaced with an Orbitrap Exploris 480 mass spectrometer (Thermo Fisher Scientific). Column
571 temperature was maintained at 60°C using a column oven (Sonation lab solutions, Biberach, DEU), and
572 peptides were separated using a binary buffer system comprising 0.1% formic acid (buffer A) and 80%
573 ACN plus 0.1% formic acid (buffer B) at a flow rate of 400 nL/min. A gradient of 3–19% buffer B was
574 employed over 40 min followed by 19–41% buffer B over 20 min, resulting in approximately 1 h
575 gradients. Peptides were analysed with one full scan (350–1,400 m/z, R = 120,000) at a target of $3e^6$
576 ions, followed by 48 data-independent acquisition MS/MS scans (350–1,022 m/z) with higher-energy
577 collisional dissociation (target $3e^6$ ions, max injection time 22 ms, isolation window 14 m/z, 1 m/z
578 window overlap, normalised collision energy 25%), and fragments were detected in the Orbitrap (R =
579 15,000).
580
581 ***MS raw data processing***
582 Raw spectral data were analysed using Spectronaut (v16.0.220606.53000). Data were searched using
583 directDIA against the Mouse UniProt Reference Proteome database (January 2022 release), with default
584 settings (precursor and protein Qvalue cutoffs 0.01, Qvalue filtering, MS2 quantification), with "PTM
585 localization" filtering turned on (threshold 0.5), and the inbuilt peptide collapse function.
586
587

588 ***Phosphoproteomics data processing***

589 Phosphopeptide intensities were log2 transformed and median normalised. Non-class I phosphopeptides
590 (localisation score ≤ 0.75) were then removed. Finally, for each phosphopeptide, outlier values were
591 removed that had a log2 intensity < 5 and were > 6 log2 intensity units lower than the phosphopeptide
592 median. Log2 fold changes between conditions were computed using condition medians.

593

594 ***Identifying insulin-regulated phosphopeptides***

595 To allow comparison across conditions, phosphopeptides were filtered for those highly quantified in
596 most strain-diet combinations. For a given phosphopeptide, this filtering was performed on two levels.
597 Firstly, each of the 10 strain-diet combinations were retained if there were ≥ 3 insulin-stimulated values
598 and ≥ 3 unstimulated values. Then, the phosphopeptide itself was retained if ≥ 8 strain-diet combinations
599 had passed the previously filtering. Phosphopeptides were then fit to a three-way ANOVA with all
600 interaction terms ("aov" in the R package "stats") and an F-test was performed assessing the main effect
601 of insulin stimulation. To correct for multiple hypothesis testing p-values were converted into q-values
602 (R package "qvalue"[71]). The log2(insulin/unstimulated) fold change with the greatest magnitude across
603 strain-diet combinations was then calculated (max log2(insulin/unstimulated)). Phosphopeptides were
604 considered "insulin-regulated" when q < 0.05 and if insulin increased or decreased phosphorylation by >
605 1.5-fold in at least one strain-diet combination (max log2(insulin/unstimulated) > 0.58 or < -0.58).

606

607 ***Calculation of insulin response values***

608 For all phosphopeptides the distribution of "insulin responses" in each strain-diet combination was
609 calculated. Specifically, within each strain-diet combination all insulin-stimulated values were
610 normalised by subtracting the unstimulated median.

611

612 ***Identifying strain and diet effects***

613 *Strain effects*

614 For each insulin-regulated phosphopeptide a one-way ANOVA was performed modelling the insulin
615 response as a function of mouse strain within the CHOW diet. p-values were converted to q-values.
616 For significant phosphopeptides (q < 0.05), t-tests were performed comparing the insulin response of
617 C57Bl6J to each of the other four strains. t-test p-values were converted to q-values and considered
618 significant when q < 0.05. To ensure that significant differences between a strain and C57Bl6J were
619 of a meaningful magnitude, the strain's log2(insulin/unstimulated) was compared to the C57Bl6J
620 log2(insulin/unstimulated). In general, if the absolute difference between the two was greater than
621 0.58 this was accepted. However, this threshold was decreased for phosphopeptides with weaker
622 insulin regulation. Specifically, the difference was retained if it passed the following filtering:

623

$$Strain\ log2(insulin/unstimulated) > f(C57Bl6J\ log2(insulin/unstimulated))$$
or
$$Strain\ log2(insulin/unstimulated) < g(C57Bl6J\ log2(insulin/unstimulated)),$$
where $f(x)$ and $g(x)$ are defined as:

$$f(x) = \left\{ \begin{array}{ll} x + 0.58, & \text{if } x \geq 2 \times 0.58 \\ \frac{5}{4}x + \frac{1}{2} \times 0.58, & \text{if } 0 \leq x < 2 \times 0.58 \\ x + \frac{1}{2} \times 0.58, & \text{if } -\frac{1}{2} \times 0.58 \leq x < 0 \\ \frac{4}{5}x + \frac{2}{5} \times 0.58, & \text{if } -3 \times 0.58 \leq x < -\frac{1}{2} \times 0.58 \\ x + 0.58, & \text{if } x < -3 \times 0.58 \end{array} \right\}$$

$$g(x) = \left\{ \begin{array}{ll} x - 0.58, & \text{if } x \geq 3 \times 0.58 \\ \frac{4}{5}x - \frac{2}{5} \times 0.58, & \text{if } \frac{1}{2} \times 0.58 \leq x < 3 \times 0.58 \\ x - \frac{1}{2} \times 0.58, & \text{if } 0 \leq x < \frac{1}{2} \times 0.58 \\ \frac{5}{4}x - \frac{1}{2} \times 0.58, & \text{if } -2 \times 0.58 \leq x < 0 \\ x - 0.58, & \text{if } x < -2 \times 0.58 \end{array} \right\}$$

An insulin-regulated phosphopeptide was considered to have a "Strain effect" if the insulin response in at least one strain was different to C57Bl6J using the q-value and log2 fold-change criteria described above.

Uniform diet and StrainxDiet effects

For each insulin-regulated phosphopeptide a two-way ANOVA was performed modelling the insulin response as a function of strain, diet, and their interaction. The p-values for the Diet and StrainxDiet terms were converted to q-values. Whenever the StrainxDiet term was significant ($q < 0.05$), additional tests were performed to identify specific strains in which the insulin response differed between CHOW and HFD. If the StrainxDiet term was not significant but the Diet term was significant, a separate filtering procedure was performed.

When the StrainxDiet term was significant, t-tests were performed to compare the CHOW insulin response to the HFD insulin response within each strain. When a t-test was significant ($q < 0.05$), the log2(insulin/unstimulated) filtering procedure described for "Strain effects" was applied comparing CHOW and HFD fold changes. Insulin-regulated phosphopeptides were considered to have a "StrainxDiet effect" if there was a difference between CHOW and HFD in at least one strain.

When only the Diet term was significant, the log2(insulin/unstimulated) filtering procedure described for "Strain effects" was applied, comparing the mean log2(insulin/unstimulated) across strains within CHOW, to the mean across HFD. Insulin-regulated phosphopeptides that passed this filter were considered to have a "Uniform diet effect".

647 ***Curated insulin signalling subnetwork***

648 A subnetwork of insulin-regulated phosphosites was curated by compiling all sites on proteins from a
649 previously published knowledge pathway-derived list of canonical insulin signalling proteins[21]. Several
650 phosphosites and proteins that were not detected as insulin regulated were included due to their
651 importance in the insulin signalling pathway. Additionally, all *in vivo* substrates of canonical insulin-
652 regulated kinases (Akt, mTOR, AMPK, Raf, Mek1/2, Erk1/2, p90RSK/Rsk2, p70S6K, Pdk1, INSR)
653 annotated in PhosphositePlus were included[32]. Annotations from orthologous phosphosites were pooled
654 across species using PhosphositePlus Site Group IDs. Phosphosite regulatory roles from
655 PhosphositePlus were indicated after manual validation by literature search. Proteins were assigned to
656 functional groups (e.g. mRNA processing, lipid metabolism) based on their Uniprot descriptions.

657

658 ***Kinase substrate enrichment analysis***

659 Kinase-substrate annotations were collated from PhosphositePlus and mapped into phosphoproteomics
660 data using Site Group IDs. Only annotations supported by *in vivo* evidence were used. Annotations for
661 kinase isoforms (e.g. Akt1, Akt2, Akt3) were merged. Substrate annotations for GSK3 were
662 supplemented with a recent list of 274 putative GSK3 substrates determined by phosphoproteomics and
663 motif analysis[31]. Autophosphorylation sites and promiscuous phosphosites targeted by ≥ 4 kinases were
664 removed. Kinase substrate enrichment analysis (KSEA) was then performed with the "ksea" function
665 from the R package "ksea"[37] (version: 0.1.2) using insulin response data and 1,000 permutations to
666 determine empirical p-values. Only phosphopeptides quantified in ≥ 50% of samples and with ≥ 1
667 insulin response value in all strain-diet combinations were used. In each sample kinases with < 5
668 quantified substrates were excluded, and only kinases with significant enrichment ($p < 0.05$) in ≥ 5
669 samples were used in subsequent analysis. To identify Strain effects on kinase activity, one-way
670 ANOVAs were performed on CHOW KSEA enrichment scores. To identify Uniform diet or
671 StrainxDiet effects, two-way ANOVAs were performed on KSEA enrichment scores testing the effects
672 of strain, diet, and their interaction. p-values were adjusted by the Benjamini-Hochberg procedure.

673

674 ***Insulin signalling subnetwork analysis***

675 Weighted gene correlation network analysis (WGCNA[39,40]) was performed with the
676 "blockwiseModules" function from the R package "WGCNA" (version 1.71) using the insulin
677 response values of all insulin-regulated phosphopeptides. Default parameters were used except for
678 power = 3 (determined as recommended in [39]), deepSplit = 3, minModuleSize = 15, reassignThreshold
679 = 0, and mergeCutHeight = 0.25. Subnetwork eigengenes were extracted and termed "eigenpeptides".

680 One-sided fisher's exact tests were performed to assess the enrichment of Gene Ontology (GO)
681 Biological Processes, GO Cellular Compartments (R package "org.Mm.eg.db" version 3.15.0[72]), and
682 kinase substrates in each subnetwork relative to the entire phosphoproteome. Only pathways containing
683 three or more subnetwork phosphoproteins were tested. Kinase substrate enrichment was performed

684 using the same annotations as KSEA. P-values were adjusted within each analysis by the Benjamini-
685 Hochberg procedure. Subnetwork phosphopeptides were mapped into insulin signalling temporal
686 clusters defined in our previous study of insulin signalling dynamics[10], using PhosphositePlus Site
687 Group IDs. The timepoint at which each cluster appeared to reach its maximum insulin-stimulated value
688 was used as a measure of insulin response speed.
689
690 ***Glucose uptake correlations***
691 For each insulin-regulated phosphopeptide, Pearson's correlation tests were performed to assess the
692 linear association between ^{3}H-2DG uptake in insulin-stimulated mice and phosphopeptide insulin
693 response values or unnormalized insulin-stimulated log2 intensity. Phosphopeptides were considered
694 correlated with ^{3}H-2DG uptake when $q < 0.1$ and their Pearson's correlation coefficient was of
695 substantial magnitude ($r > 0.35$ or $r < -0.35$). Pearson's correlation tests were also performed comparing
696 insulin-stimulated ^{3}H-2DG uptake to KSEA enrichment scores in individual mice or using the median
697 in each strain-diet combination.
698
699 ***Cell culture***
700 GLUT4-HA-L6 myoblasts[73] were grown in α-MEM supplemented with 10% fetal bovine serum in a
701 humidified chamber at 37 °C, 10% CO2. Differentiation was induced by changing media to α-MEM
702 supplemented with 2% horse serum for 5 days.
703
704 ***PFKFB3 overexpression***
705 Platinum-E (Plat-E) retroviral packaging cells were grown to confluency and transfected with 10 µg
706 total DNA: either pBabe puromycin empty vector, pBabe puromycin PFKFB3 or pWZL neomycin HA-
707 GLUT4. After 48 h retroviral media was collected and passed through a 0.45 µm filter. L6 myotubes
708 were grown to confluence and retrovirally transfected with 2 mL of HA-GLUT4 neomycin viral media
709 in the presence of 10 µg/ml polybrene. The following morning, cells were split into growth media
710 containing neomycin (800 µg/ml) and passaged until only successfully transfected cells remained.
711 These cells were then grown to confluence and retrovirally transfected again with 2 mL of either empty
712 vector puromycin viral media or PFKFB3 puromycin viral media in the presence of 10 µg/ml of
713 polybrene. The following morning, cells were split into growth media containing both neomycin (800
714 µg/ml) and puromycin (2 µg/ml) and passaged until only successfully transfected cells remained in
715 culture.
716
717 ***Immunoblotting***
718 GLUT4-HA-L6 myotubes were incubated overnight (16 h) in either BSA-conjugated 125 µM palmitate
719 or BSA vehicle control. Cells were then washed in ice-cold PBS and lysed by scraping directly into
720 55 °C Laemmli sample buffer with 10 % (tris 2-carboxyethyl phosphine; TCEP). Samples were

721 sonicated for 24 s (3s on/3s off) and heated at 65 °C for 5 minutes. Samples were then resolved by SDS-
722 PAGE as previously described[17], transferred onto PVDF membranes and blocked in TBS-T (0.1%
723 Tween in Tris-buffered saline) containing 5% skim milk for 1 h. Membranes were then washed 3 x 10
724 min in TBS-T and incubated overnight in primary antibodies against Pfkfb3 (Proteintech Group; 13763-
725 1-AP) and α-tubulin (Cell Signalling Technologies #2125; diluted 1:1000). The following day
726 membranes were washed 3 x 10 min in TBS-T and incubated for 1 h in species-appropriate fluorescent
727 antibodies. Imaging and densitometry were performed using LI-COR Image Studio.
728
729 ***Extracellular acidification rate***
730 The extracellular acidification rate (ECAR) of GLUT4-HA-L6 cells myotubes was measured using
731 Seahorse XFp miniplates and a Seahorse XF HS Mini Analyzer (Seahorse Bioscience, Copenhagen,
732 Denmark) as previously described[74]. Cells incubated in palmitate or BSA control were washed twice
733 with Krebs-Ringer Bicarbonate Buffer (Sigma, K4002) and once with standard cell culture media
734 without bicarbonate (XF-DMEM, pH 7.4). Cells were then incubated in XF-DMEM without glucose
735 at 37°C for 1 h in a non-CO2 incubator, followed by assaying in the XFp Analyzer. ECAR was
736 measured after a 12-minute equilibration period followed by mix/wait/read cycles of 3/0/3 min. After
737 stabilizing the baseline rates, compounds were injected to reach a final concentration of: 10 mM
738 glucose, 5 µg/mL oligomycin, and 50 mM 2-deoxyglucose (2-DG), allowing estimation of glucose-
739 driven glycolysis (glucose ECAR - basal ECAR), glycolytic capacity (oligomycin ECAR - 2DG
740 ECAR), and non-glycolytic acidification (equal to 2DG ECAR). Data were normalized to protein
741 concentration and presented as a percentage of total ECAR.
742
743 ***2DG uptake in GLUT4-HA-L6 myotubes***
744 2-deoxyglucose (2DG) uptake into GLUT4-HA-L6 myotubes was performed as previously described
745 with modifications[73,75]. Cells were incubated overnight in αMEM supplemented with either BSA-
746 coupled 125 µM palmitic acid or BSA vehicle control before being washed 3x with 37 °C HEPES-
747 buffered saline (HBS). Cells were then incubated in HBS supplemented with 10 µM unlabelled 2-
748 deoxyglucose and either 0 or 100 nM insulin at 37°C for 15 min. Cells were then incubated for a further
749 5 min following the addition of 0.5 µCi/ml [^{3}H]-2-deoxyglucose in HBS. Cells were then washed on
750 ice 5x with ice-cold PBS and lysed in 1 M NaOH. For non-specific background uptake, 1 well per
751 condition was pre-treated with cytochalasin B. Counts were determined by Perkin Elmer Quantulus
752 GCT Liquid Scintillation Counter (Perkin Elmer, Waltham, MA, USA). 2DG uptake was expressed
753 relatively to protein concentration as determined by bicinchoninic acid (BCA) assay after neutralisation
754 with 1 M HCl and subtraction of non-specific uptake.
755
756

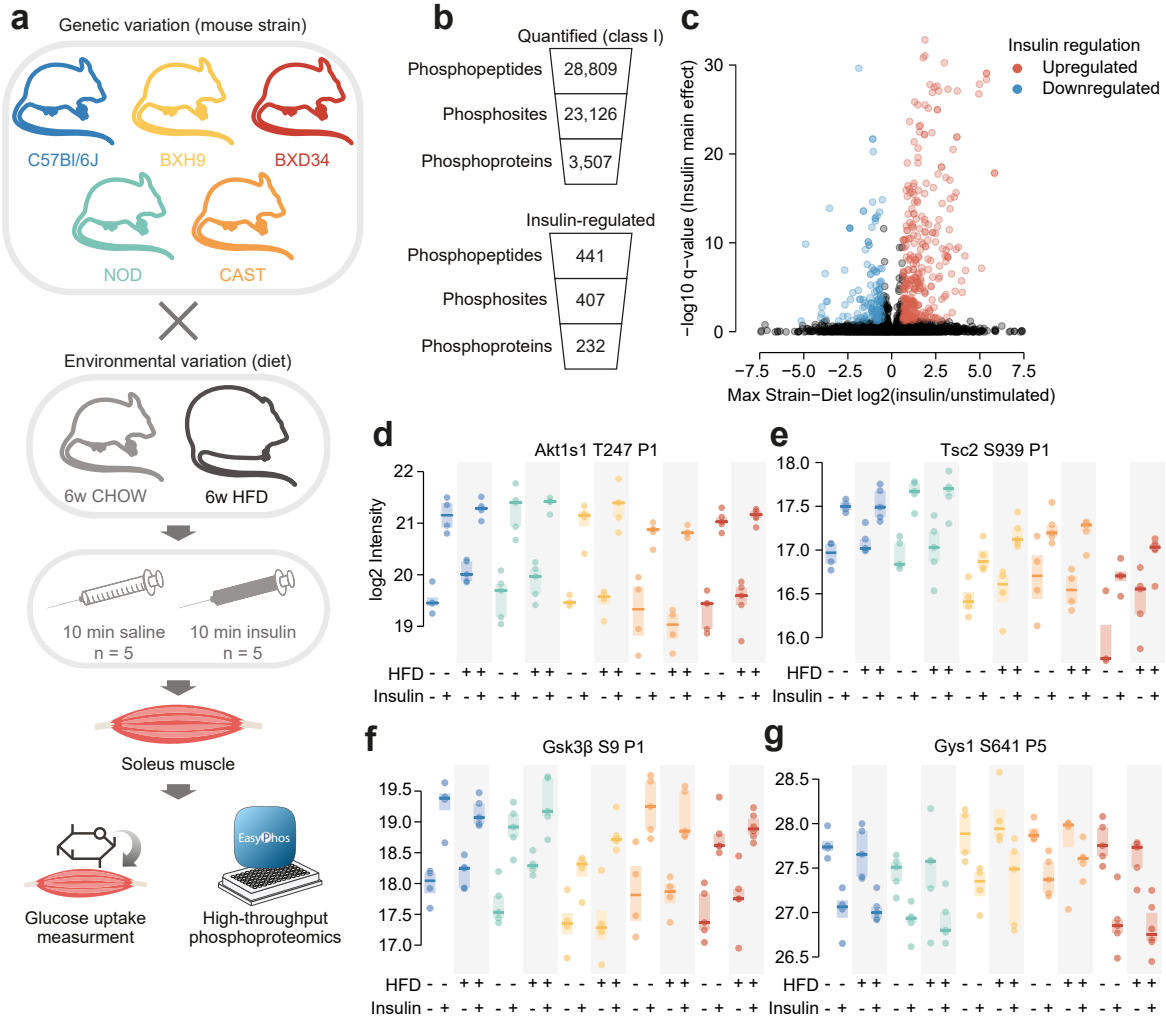

Figure 1: Phosphoproteomics of insulin signalling in mouse skeletal muscle. a) Workflow for skeletal muscle phosphoproteomics of insulin signalling. **b)** Quantification of skeletal muscle phosphoproteomics. **c)** Volcano plot identifying insulin-regulated phosphopeptides. The greatest log2(insulin/unstimulated) fold change across strain-diet combinations is plotted against significance (insulin stimulation main effect, three-way ANOVA). Three phosphopeptides with -log10 q-values greater than 35 were removed for visual clarity. **d-g)** Example insulin-regulated phosphopeptides. The protein and phosphorylated amino acid are indicated, as well as the number of phosphosites on the phosphopeptide (e.g. "P1"). n = 4-6 biological replicates.

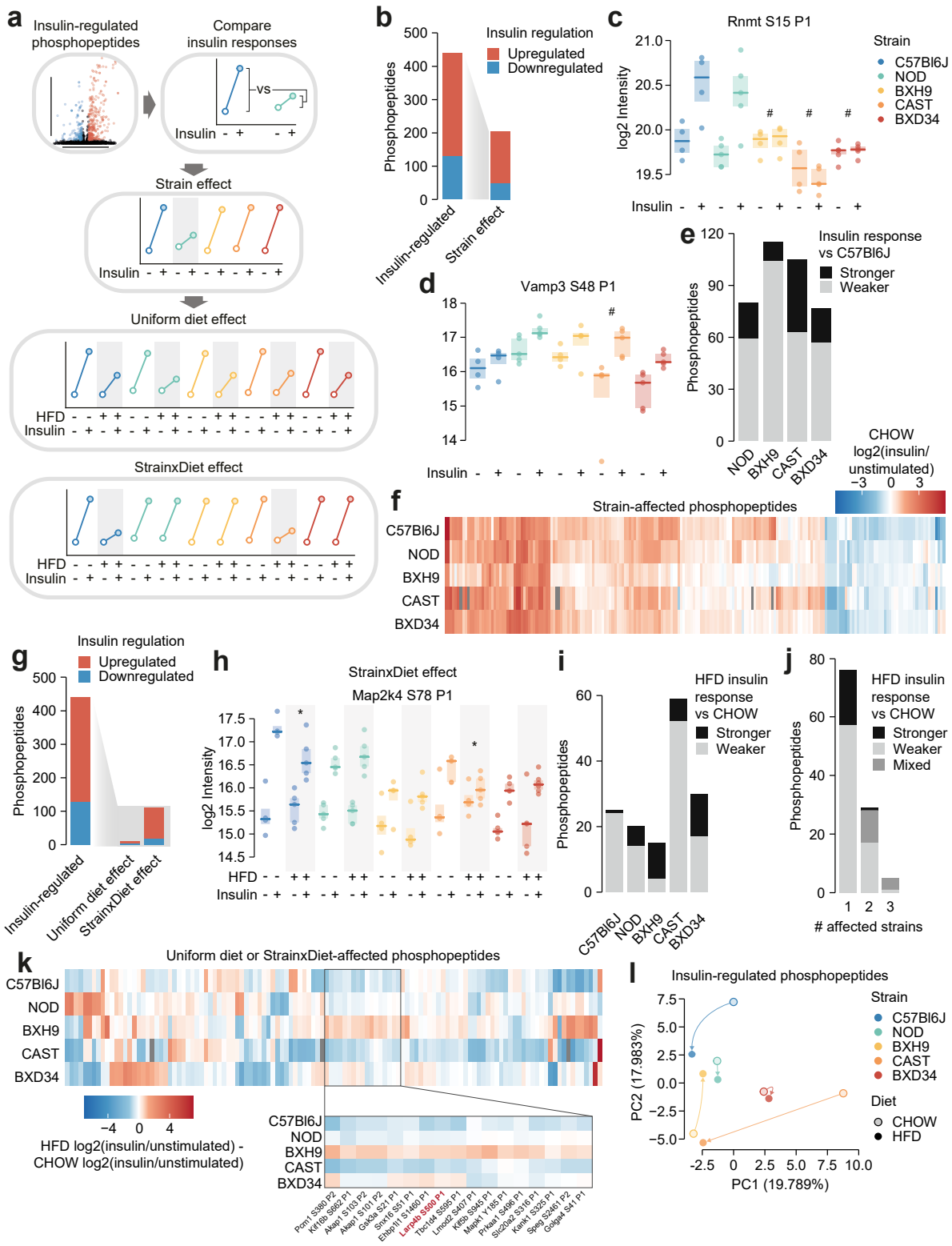

Figure 2: Genetics and diet modulate insulin signalling. a) Schematic for identifying effects of strain and diet on insulin signalling. **b)** The number of total insulin-regulated phosphopeptides and those with a Strain effect. **c-d)** Two phosphopeptides with Strain effects. ANOVAs were performed on CHOW insulin responses following two-sided t-tests comparing each strain to C57Bl6J (q-values: #). Only CHOW values are shown. **e)** The number of phosphopeptides with stronger or weaker insulin regulation in each strain compared to C57Bl6J. **f)** Heatmap displaying all insulin-regulated phosphopeptides with a Strain effect. Missing values are coloured

grey. **g)** The number of total insulin-regulated phosphopeptides and those with diet effects. **h)** A phosphopeptide with a StrainxDiet effect. A two-way ANOVA was performed on insulin response values followed by two-sided t-tests comparing HFD to CHOW within each strain (q-values: *). **i-j)** The number of phosphopeptides with a StrainxDiet effect in **i)** each strain, or **j)** each number of strains. Colour indicates whether the insulin response in HFD is stronger vs CHOW, weaker vs CHOW, or both in different strains ("Mixed"). **k)** Heatmap displaying all insulin-regulated phosphopeptides with a Uniform diet effect or StrainxDiet effect. Inset displays example sites where BXH9 effects contrasted other strains. **l)** PCA of all insulin-regulated phosphopeptides using the log2(insulin/unstimulated) fold changes for each Strain-Diet combination. The percentage of total variance explained by each principal component is indicated. */#: $0.01 \leq q < 0.05$, **/##: $0.001 \leq q < 0.01$, ***/###: $q < 0.001$. n = 4-6 biological replicates.

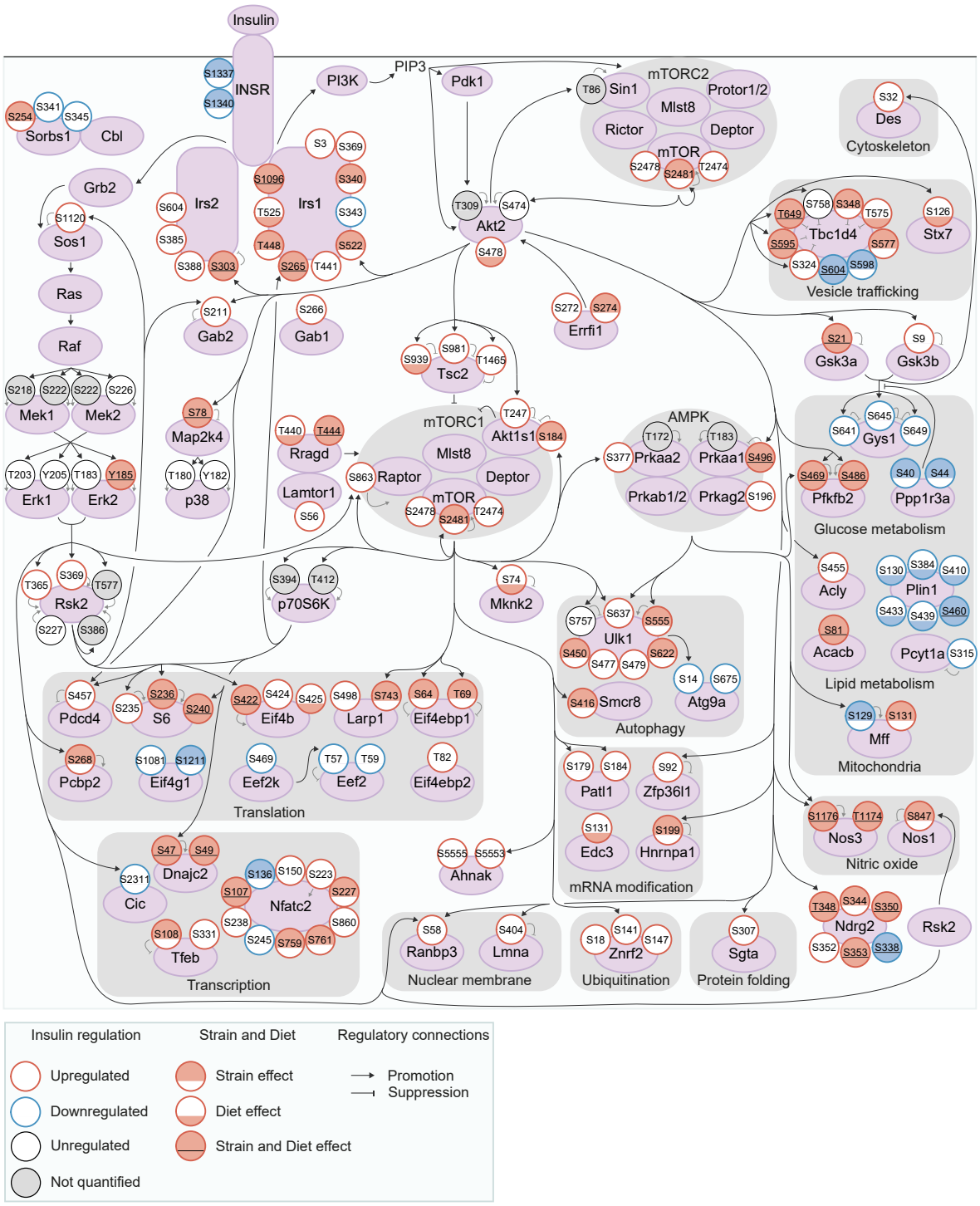

Figure 3: Exploring genetic and dietary modulation of the insulin signalling network. A curated network of 160 insulin-regulated phosphosites. Phosphosites are depicted as circles where the outline colour denotes the direction of insulin regulation, and the inner colour denotes the presence of Strain effects or Diet effects (either a StrainxDiet or Uniform diet effect). Black arrows indicate regulatory relationships from proteins to other proteins or phosphosites. Grey lines indicate phosphosite regulatory roles.

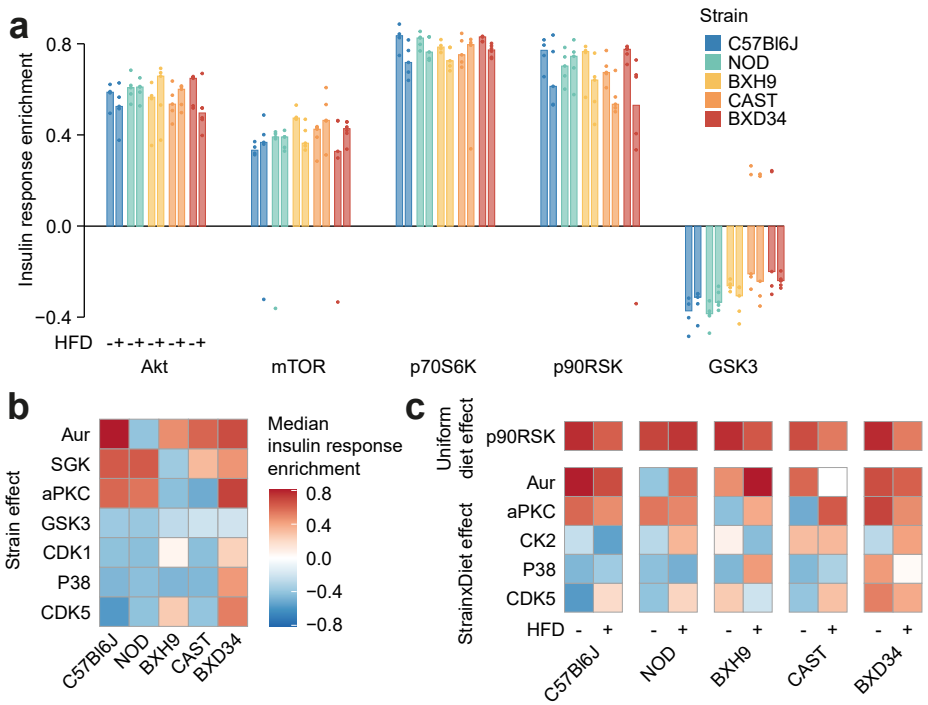

Figure 4: Genetics and diet rewire insulin-regulated kinase signalling. a) Kinase substrate enrichment analysis (KSEA)[37] of five canonical insulin-regulated kinases using insulin response values and kinase-substrate annotations from PhosphositePlus[32]. **b-c)** Kinase enrichment scores were tested for **b)** Strain effects (CHOW ANOVA adjusted $p < 0.05$) or **c)** StrainxDiet effects (two-way ANOVA interaction effect adjusted $p < 0.05$) and Uniform diet effects (Diet main effect adjusted $p < 0.05$, interaction effect adjusted $p \geq 0.05$). n = 4-6 biological replicates.

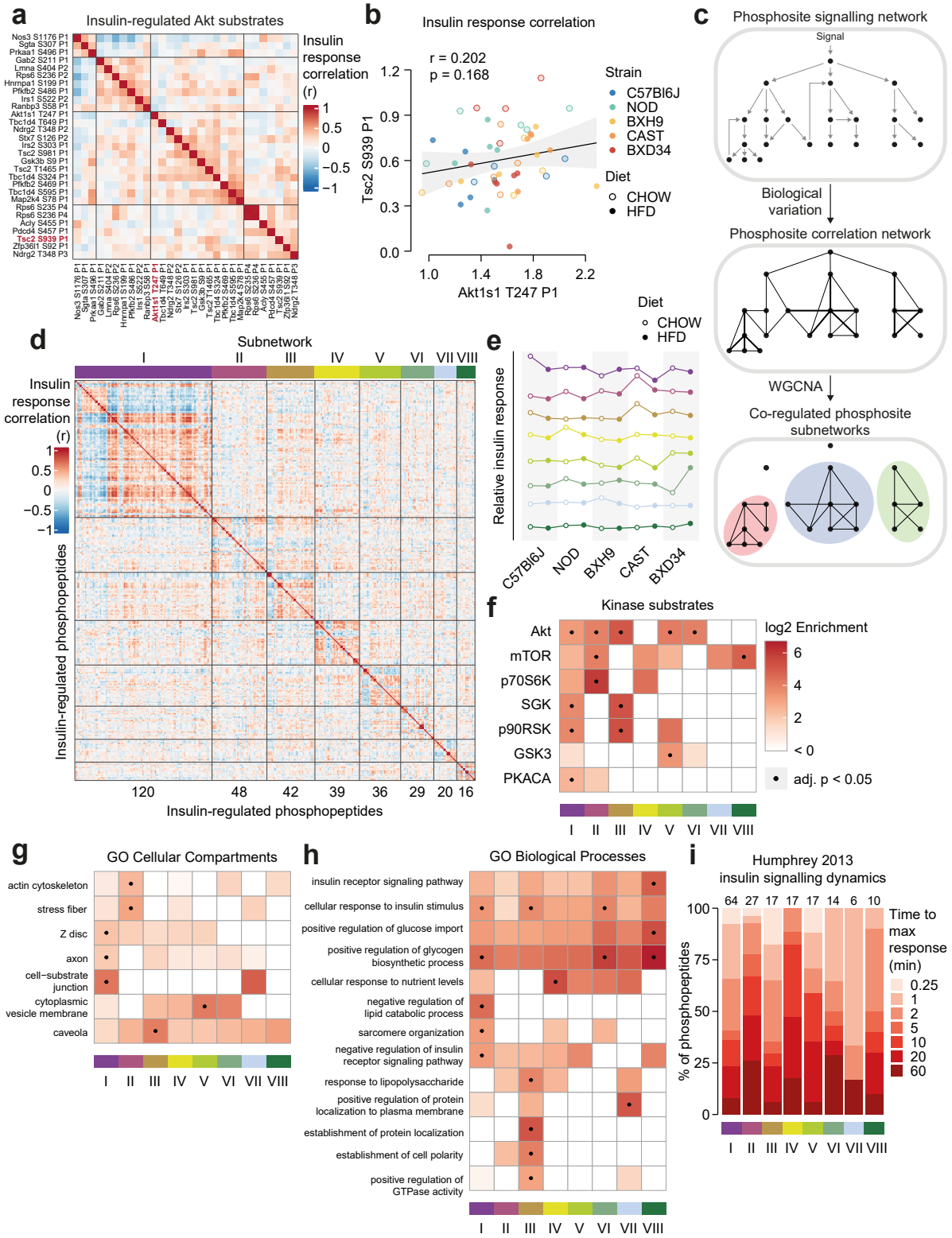

Figure 5: Biological variation reveals functional organisation of the insulin signalling network. **a)** Pairwise Pearson's correlation of the insulin response values of insulin-regulated Akt substrates. Substrates were separated into four clusters by hierarchical clustering followed by tree cutting. **b)** The correlation between insulin response values of the Akt substrates Tsc2 S939 and Akt1s1 T247. Linear regression is indicated with 95% confidence intervals. **c)** Rationale for performing WGCNA. **d)** Pairwise Pearson's correlation of all insulin-regulated phosphopeptides separated into WGCNA-derived subnetworks. The number of

phosphopeptides in each subnetwork is indicated below the heatmap. **e)** The "eigenpeptide" of each subnetwork. The median of each strain-diet combination is shown. **f-h)** The enrichment of **f)** PhosphositePlus-derived kinase-substrate annotations[32], **g)** GO cellular compartments, and **h)** GO biological processes within each subnetwork relative to the entire phosphoproteome (one-sided Fisher's exact test, Benjamini-Hochberg p-value adjustment). **i)** The time taken for phosphopeptides to reach maximum insulin-stimulated intensity in a previous study of insulin signalling dynamics[10]. The number of phosphopeptides mapped into the study is indicated above each bar.

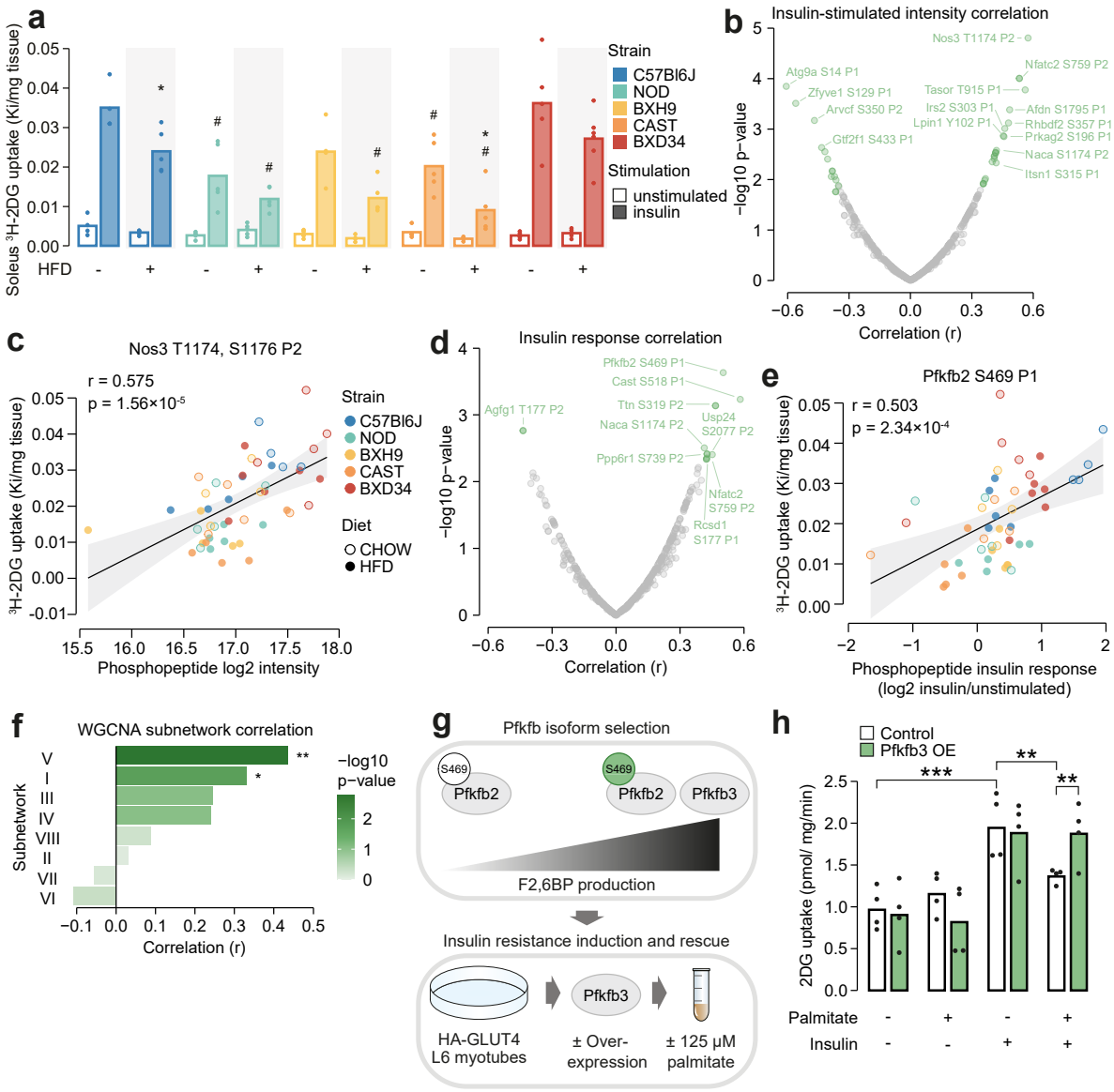

Figure 6: Leveraging biological variation to identify drivers of insulin responsiveness. a) The uptake of ^{3}H-2DG into mouse soleus muscle after a 10 min injection of insulin (1 U/kg lean mass; "insulin") or saline ("unstimulated") calculated as a rate constant (Ki). Two-sided t-tests were performed on insulin-stimulated uptake values to compare HFD to CHOW within each strain (adjusted p-value: *) or each strain to C57Bl6J within either diet (adjusted p-value: #). n = 4-6 biological replicates. **b)** Pearson's correlation between log2 intensity of insulin-regulated phosphopeptides and ^{3}H-2DG uptake within insulin-stimulated mice. Significantly correlated phosphopeptides (q-value < 0.1, r > 0.35 or r < -0.35) are coloured green and select correlated phosphopeptides are labelled. **c)** Correlation of Nos3 T1174, S1176 insulin-stimulated intensity with insulin-stimulated ^{3}H-2DG uptake. Linear regression is indicated with 95% confidence intervals. **d)** As in **b)**, using phosphopeptide insulin response values. **e)** Correlation of the Pfkfb2 S469 insulin response with insulin-stimulated ^{3}H-2DG uptake. **f)** Correlation of WGCNA subnetwork eigenpeptides with insulin-stimulated ^{3}H-2DG uptake. Significant correlations are indicated (*). **g)** Rationale and workflow for over-expressing Pfkfb3 to rescue palmitate-induced insulin resistance. **h)** Unstimulated and insulin-stimulated glucose uptake (100 nM insulin) in L6-GLUT4-HA myotubes. A two-way repeated measures ANOVA was performed followed by

Tukey's posthoc tests (*). Not all significant comparisons are shown. n = 4 biological replicates. */#: $0.01 \leq p < 0.05$, **/##: $0.001 \leq p < 0.01$, ***/###: $p < 0.001$

References

1. Humphrey, S.J., James, D.E., and Mann, M. (2015). Protein Phosphorylation: A Major Switch Mechanism for Metabolic Regulation. Trends Endocrinol. Metab. *26*, 676–687.

2. Needham, E.J., Parker, B.L., Burykin, T., James, D.E., and Humphrey, S.J. (2019). Illuminating the dark phosphoproteome. Sci. Signal. *12*. 10.1126/scisignal.aau8645.

3. Olsen, J.V., Blagoev, B., Gnad, F., Macek, B., Kumar, C., Mortensen, P., and Mann, M. (2006). Global, in vivo, and site-specific phosphorylation dynamics in signaling networks. Cell *127*, 635–648.

4. Bodenmiller, B., Wanka, S., Kraft, C., Urban, J., Campbell, D., Pedrioli, P.G., Gerrits, B., Picotti, P., Lam, H., Vitek, O., Brusniak, M.-Y., Roschitzki, B., Zhang, C., Shokat, K.M., Schlapbach, R., Colman-Lerner, A., Nolan, G.P., Nesvizhskii, A.I., Peter, M., Loewith, R., von Mering, C., and Aebersold, R. (2010). Phosphoproteomic analysis reveals interconnected system-wide responses to perturbations of kinases and phosphatases in yeast. Sci. Signal. *3*, rs4.

5. Needham, E.J., Humphrey, S.J., Cooke, K.C., Fazakerley, D.J., Duan, X., Parker, B.L., and James, D.E. (2019). Phosphoproteomics of Acute Cell Stressors Targeting Exercise Signaling Networks Reveal Drug Interactions Regulating Protein Secretion. Cell Rep. *29*, 1524-1538.e6.

6. Leutert, M., Barente, A.S., Fukuda, N.K., Rodriguez-Mias, R.A., and Villén, J. (2022). The regulatory landscape of the yeast phosphoproteome. bioRxiv, 2022.10.23.513432. 10.1101/2022.10.23.513432.

7. Haeusler, R.A., McGraw, T.E., and Accili, D. (2018). Biochemical and cellular properties of insulin receptor signalling. Nat. Rev. Mol. Cell Biol. *19*, 31–44.

8. Gehart, H., Kumpf, S., Ittner, A., and Ricci, R. (2010). MAPK signalling in cellular metabolism: stress or wellness? EMBO Rep. *11*, 834–840.

9. Sylow, L., Jensen, T.E., Kleinert, M., Højlund, K., Kiens, B., Wojtaszewski, J., Prats, C., Schjerling, P., and Richter, E.A. (2013). Rac1 signaling is required for insulin-stimulated glucose uptake and is dysregulated in insulin-resistant murine and human skeletal muscle. Diabetes *62*, 1865–1875.

10. Humphrey, S.J., Yang, G., Yang, P., Fazakerley, D.J., Stöckli, J., Yang, J.Y., and James, D.E. (2013). Dynamic adipocyte phosphoproteome reveals that Akt directly regulates mTORC2. Cell Metab. *17*, 1009–1020.

11. Humphrey, S.J., Azimifar, S.B., and Mann, M. (2015). High-throughput phosphoproteomics reveals in vivo insulin signaling dynamics. Nat. Biotechnol. *33*, 990–995.

12. Krüger, M., Kratchmarova, I., Blagoev, B., Tseng, Y.-H., Kahn, C.R., and Mann, M. (2008). Dissection of the insulin signaling pathway via quantitative phosphoproteomics. Proc. Natl. Acad. Sci. U. S. A. *105*, 2451–2456.

13. James, D.E., Stöckli, J., and Birnbaum, M.J. (2021). The aetiology and molecular landscape of insulin resistance. Nat. Rev. Mol. Cell Biol. 10.1038/s41580-021-00390-6.

14. Fazakerley, D.J., Krycer, J.R., Kearney, A.L., Hocking, S.L., and James, D.E. (2019). Muscle and adipose tissue insulin resistance: malady without mechanism? J. Lipid Res. *60*, 1720–1732.

15. Hunter, D.J. (2005). Gene–environment interactions in human diseases. Nat. Rev. Genet. *6*, 287–298.

16. Civelek, M., and Lusis, A.J. (2014). Systems genetics approaches to understand complex traits. Nat. Rev. Genet. *15*, 34–48.

17. Nelson, M.E., Madsen, S., Cooke, K.C., Fritzen, A.M., Thorius, I.H., Masson, S.W.C., Carroll, L., Weiss, F.C., Seldin, M.M., Potter, M., Hocking, S.L., Fazakerley, D.J., Brandon, A.E., Thillainadesan, S., Senior, A.M., Cooney, G.J., Stöckli, J., and James, D.E. (2022). Systems-level analysis of insulin action in mouse strains provides insight into tissue- and pathway-specific interactions that drive insulin resistance. Cell Metab. *34*, 227-239.e6.

18. Montgomery, M.K., Hallahan, N.L., Brown, S.H., Liu, M., Mitchell, T.W., Cooney, G.J., and Turner, N. (2013). Mouse strain-dependent variation in obesity and glucose homeostasis in response to high-fat feeding. Diabetologia *56*, 1129–1139.

19. Grossbach, J., Gillet, L., Clément-Ziza, M., Schmalohr, C.L., Schubert, O.T., Schütter, M., Mawer, J.S.P., Barnes, C.A., Bludau, I., Weith, M., Tessarz, P., Graef, M., Aebersold, R., and Beyer, A. (2022). The impact of genomic variation on protein phosphorylation states and regulatory networks. Mol. Syst. Biol. *18*, e10712.

20. Zhang, T., Keele, G.R., Gyuricza, I.G., Vincent, M., Brunton, C., Bell, T.A., Hock, P., Shaw, G.D., Munger, S.C., de Villena, F.P.-M., Ferris, M.T., Paulo, J.A., Gygi, S.P., and Churchill, G.A. (2023). Multi-omics analysis identifies drivers of protein phosphorylation. Genome Biol. *24*, 52.

21. Needham, E.J., Hingst, J.R., Parker, B.L., Morrison, K.R., Yang, G., Onslev, J., Kristensen, J.M., Højlund, K., Ling, N.X.Y., Oakhill, J.S., Richter, E.A., Kiens, B., Petersen, J., Pehmøller, C., James, D.E., Wojtaszewski, J.F.P., and Humphrey, S.J. (2021). Personalized phosphoproteomics identifies functional signaling. Nat. Biotechnol. 10.1038/s41587-021-01099-9.

22. McCarthy, M.I., Abecasis, G.R., Cardon, L.R., Goldstein, D.B., Little, J., Ioannidis, J.P.A., and Hirschhorn, J.N. (2008). Genome-wide association studies for complex traits: consensus, uncertainty and challenges. Nat. Rev. Genet. *9*, 356–369.

23. Lusis, A.J., Seldin, M.M., Allayee, H., Bennett, B.J., Civelek, M., Davis, R.C., Eskin, E., Farber, C.R., Hui, S., Mehrabian, M., Norheim, F., Pan, C., Parks, B., Rau, C.D., Smith, D.J., Vallim, T., Wang, Y., and Wang, J. (2016). The Hybrid Mouse Diversity Panel: a resource for systems genetics analyses of metabolic and cardiovascular traits. J. Lipid Res. *57*, 925–942.

24. Burchfield, J.G., Kebede, M.A., Meoli, C.C., Stöckli, J., Tess Whitworth, P., Wright, A.L., Hoffman, N.J., Minard, A.Y., Ma, X., Krycer, J.R., Nelson, M.E., Tan, S.-X., Yau, B., Thomas, K.C., Wee, N.K.Y., Khor, E.-C., Enriquez, R.F., Vissel, B., Biden, T.J., Baldock, P.A., Hoehn, K.L., Cantley, J., Cooney, G.J., James, D.E., and Fazakerley, D.J. (2018). High dietary fat and sucrose result in an extensive and time-dependent deterioration in health of multiple physiological systems in mice. J. Biol. Chem. *293*, 5731–5745.

25. DeFronzo, R.A. (1988). The Triumvirate: β-Cell, Muscle, Liver: A Collusion Responsible for NIDDM. Diabetes *37*, 667–687.

26. Schiaffino, S., and Reggiani, C. (2011). Fiber types in mammalian skeletal muscles. Physiol. Rev. *91*, 1447–1531.

27. Humphrey, S.J., Karayel, O., James, D.E., and Mann, M. (2018). High-throughput and high-sensitivity phosphoproteomics with the EasyPhos platform. Nat. Protoc. *13*, 1897–1916.

28. Bekker-Jensen, D.B., Bernhardt, O.M., Hogrebe, A., Martinez-Val, A., Verbeke, L., Gandhi, T., Kelstrup, C.D., Reiter, L., and Olsen, J.V. (2020). Rapid and site-specific deep phosphoproteome profiling by data-independent acquisition without the need for spectral libraries. Nat. Commun. *11*, 787.

29. Batista, T.M., Jayavelu, A.K., Wewer Albrechtsen, N.J., Iovino, S., Lebastchi, J., Pan, H., Dreyfuss, J.M., Krook, A., Zierath, J.R., Mann, M., and Kahn, C.R. (2020). A Cell-Autonomous Signature of Dysregulated Protein Phosphorylation Underlies Muscle Insulin Resistance in Type 2 Diabetes. Cell Metab. *32*, 844-859.e5.

30. Haider, N., Lebastchi, J., Jayavelu, A.K., Batista, T.M., Pan, H., Dreyfuss, J.M., Carcamo-Orive, I., Knowles, J.W., Mann, M., and Kahn, C.R. (2021). Signaling defects associated with insulin resistance in non-diabetic and diabetic individuals and modification by sex. J. Clin. Invest. 10.1172/JCI151818.

31. Fazakerley, D.J., van Gerwen, J., Cooke, K.C., Duan, X., Needham, E.J., Díaz-Vegas, A., Madsen, S., Norris, D.M., Shun-Shion, A.S., Krycer, J.R., Burchfield, J.G., Yang, P., Wade, M.R., Brozinick, J.T., James, D.E., and Humphrey, S.J. (2023). Phosphoproteomics reveals rewiring of the insulin signaling network and multi-nodal defects in insulin resistance. Nat. Commun. *14*, 1–20.

32. Hornbeck, P.V., Zhang, B., Murray, B., Kornhauser, J.M., Latham, V., and Skrzypek, E. (2015). PhosphoSitePlus, 2014: mutations, PTMs and recalibrations. Nucleic Acids Res. *43*, D512-20.

33. Ochoa, D., Jarnuczak, A.F., Viéitez, C., Gehre, M., Soucheray, M., Mateus, A., Kleefeldt, A.A., Hill, A., Garcia-Alonso, L., Stein, F., Krogan, N.J., Savitski, M.M., Swaney, D.L., Vizcaíno, J.A., Noh, K.-M., and Beltrao, P. (2020). The functional landscape of the human phosphoproteome. Nat. Biotechnol. *38*, 365–373.

34. Schwenk, R.W., Angin, Y., Steinbusch, L.K.M., Dirkx, E., Hoebers, N., Coumans, W.A., Bonen, A., Broers, J.L.V., van Eys, G.J., Glatz, J.F.C., and Others (2012). Overexpression of vesicle-associated membrane protein (VAMP) 3, but not VAMP2, protects glucose transporter (GLUT) 4 protein translocation in an in vitro model of cardiac insulin resistance. J. Biol. Chem. *287*, 37530–37539.

35. Barilari, M., Bonfils, G., Treins, C., Koka, V., De Villeneuve, D., Fabrega, S., and Pende, M. (2017). ZRF1 is a novel S6 kinase substrate that drives the senescence programme. EMBO J. *36*, 736–750.

36. Agassandian, M., Zhou, J., Tephly, L.A., Ryan, A.J., Carter, A.B., and Mallampalli, R.K. (2005). Oxysterols inhibit phosphatidylcholine synthesis via ERK docking and phosphorylation of CTP:phosphocholine cytidylyltransferase. J. Biol. Chem. *280*, 21577–21587.

37. Hernandez-Armenta, C., Ochoa, D., Gonçalves, E., Saez-Rodriguez, J., and Beltrao, P. (2017). Benchmarking substrate-based kinase activity inference using phosphoproteomic data. Bioinformatics *33*, 1845–1851.

38. Tonks, K.T., Ng, Y., Miller, S., Coster, A.C.F., Samocha-Bonet, D., Iseli, T.J., Xu, A., Patrick, E., Yang, J.Y.H., Junutula, J.R., Modrusan, Z., Kolumam, G., Stöckli, J., Chisholm, D.J., James, D.E., and Greenfield, J.R. (2013). Impaired Akt phosphorylation in insulin-resistant human muscle is accompanied by selective and heterogeneous downstream defects. Diabetologia *56*, 875–885.

39. Zhang, B., and Horvath, S. (2005). A General Framework for Weighted Gene Co-Expression Network Analysis. Statistical Applications in Genetics and Molecular Biology *4*. 10.2202/1544-6115.1128.

40. Langfelder, P., and Horvath, S. (2008). WGCNA: an R package for weighted correlation network analysis. BMC Bioinformatics *9*, 559.

41. Roy, D., Perreault, M., and Marette, A. (1998). Insulin stimulation of glucose uptake in skeletal muscles and adipose tissues in vivo is NO dependent. Am. J. Physiol. *274*, E692-9.

887 42. Bahadoran, Z., Mirmiran, P., and Ghasemi, A. (2020). Role of Nitric Oxide in Insulin Secretion
888 and Glucose Metabolism. Trends Endocrinol. Metab. *31*, 118–130.

889 43. Dimmeler, S., Fleming, I., Fisslthaler, B., Hermann, C., Busse, R., and Zeiher, A.M. (1999).
890 Activation of nitric oxide synthase in endothelial cells by Akt-dependent phosphorylation. Nature
891 *399*, 601–605.

892 44. Lundh, M., Petersen, P.S., Isidor, M.S., Kazoka-Sørensen, D.N., Plucińska, K., Shamsi, F., Ørskov,
893 C., Tozzi, M., Brown, E.L., Andersen, E., Ma, T., Müller, U., Barrès, R., Kristiansen, V.B.,
894 Gerhart-Hines, Z., Tseng, Y.-H., and Emanuelli, B. (2019). Afadin is a scaffold protein repressing
895 insulin action via HDAC6 in adipose tissue. EMBO Rep. *20*, e48216.

896 45. O'Neill, H.M. (2013). AMPK and Exercise: Glucose Uptake and Insulin Sensitivity. Diabetes
897 Metab. J. *37*, 1–21.

898 46. Deprez, J., Vertommen, D., Alessi, D.R., Hue, L., and Rider, M.H. (1997). Phosphorylation and
899 activation of heart 6-phosphofructo-2-kinase by protein kinase B and other protein kinases of the
900 insulin signaling cascades. J. Biol. Chem. *272*, 17269–17275.

901 47. Marsin, A.-S., Bertrand, L., Rider, M.H., Deprez, J., Beauloye, C., Vincent, M.F., Van den Berghe,
902 G., Carling, D., and Hue, L. (2000). Phosphorylation and activation of heart PFK-2 by AMPK has
903 a role in the stimulation of glycolysis during ischaemia. Curr. Biol. *10*, 1247–1255.

904 48. Ros, S., and Schulze, A. (2013). Balancing glycolytic flux: the role of 6-phosphofructo-2-
905 kinase/fructose 2,6-bisphosphatases in cancer metabolism. Cancer Metab *1*, 8.

906 49. Stöckli, J., Fazakerley, D.J., and James, D.E. (2011). GLUT4 exocytosis. J. Cell Sci. *124*, 4147–
907 4159.

908 50. Dokken, B.B., Sloniger, J.A., and Henriksen, E.J. (2005). Acute selective glycogen synthase
909 kinase-3 inhibition enhances insulin signaling in prediabetic insulin-resistant rat skeletal muscle.
910 Am. J. Physiol. Endocrinol. Metab. *288*, E1188-94.

911 51. Henriksen, E.J., and Teachey, M.K. (2007). Short-term in vitro inhibition of glycogen synthase
912 kinase 3 potentiates insulin signaling in type I skeletal muscle of Zucker Diabetic Fatty rats.
913 Metabolism *56*, 931–938.

914 52. Ring, D.B., Johnson, K.W., Henriksen, E.J., Nuss, J.M., Goff, D., Kinnick, T.R., Ma, S.T., Reeder,
915 J.W., Samuels, I., Slabiak, T., Wagman, A.S., Hammond, M.-E.W., and Harrison, S.D. (2003).
916 Selective glycogen synthase kinase 3 inhibitors potentiate insulin activation of glucose transport
917 and utilization in vitro and in vivo. Diabetes *52*, 588–595.

918 53. Trefely, S., Khoo, P.-S., Krycer, J.R., Chaudhuri, R., Fazakerley, D.J., Parker, B.L., Sultani, G.,
919 Lee, J., Stephan, J.-P., Torres, E., Jung, K., Kuijl, C., James, D.E., Junutula, J.R., and Stöckli, J.
920 (2015). Kinome Screen Identifies PFKFB3 and Glucose Metabolism as Important Regulators of
921 the Insulin/Insulin-like Growth Factor (IGF)-1 Signaling Pathway. J. Biol. Chem. *290*, 25834–
922 25846.

923 54. Hoehn, K.L., Salmon, A.B., Hohnen-Behrens, C., Turner, N., Hoy, A.J., Maghzal, G.J., Stocker,
924 R., Van Remmen, H., Kraegen, E.W., Cooney, G.J., Richardson, A.R., and James, D.E. (2009).
925 Insulin resistance is a cellular antioxidant defense mechanism. Proc. Natl. Acad. Sci. U. S. A. *106*,
926 17787–17792.

927 55. Bloom, J., and Cross, F.R. (2007). Multiple levels of cyclin specificity in cell-cycle control. Nat.
928 Rev. Mol. Cell Biol. *8*, 149–160.

929 56. Steinberg, G.R., and Hardie, D.G. (2023). New insights into activation and function of the AMPK.
930 Nat. Rev. Mol. Cell Biol. *24*, 255–272.

931 57. Lavoie, H., Gagnon, J., and Therrien, M. (2020). ERK signalling: a master regulator of cell
932 behaviour, life and fate. Nat. Rev. Mol. Cell Biol. *21*, 607–632.

933 58. Meyuhas, O. (2015). Ribosomal Protein S6 Phosphorylation: Four Decades of Research. Int. Rev.
934 Cell Mol. Biol. *320*, 41–73.

935 59. Johnson, J.L., Yaron, T.M., Huntsman, E.M., Kerelsky, A., Song, J., Regev, A., Lin, T.-Y.,
936 Liberatore, K., Cizin, D.M., Cohen, B.M., Vasan, N., Ma, Y., Krismer, K., Robles, J.T., van de
937 Kooij, B., van Vlimmeren, A.E., Andrée-Busch, N., Käufer, N.F., Dorovkov, M.V., Ryazanov,
938 A.G., Takagi, Y., Kastenhuber, E.R., Goncalves, M.D., Hopkins, B.D., Elemento, O., Taatjes, D.J.,
939 Maucuer, A., Yamashita, A., Degterev, A., Uduman, M., Lu, J., Landry, S.D., Zhang, B.,
940 Cossentino, I., Linding, R., Blenis, J., Hornbeck, P.V., Turk, B.E., Yaffe, M.B., and Cantley, L.C.
941 (2023). An atlas of substrate specificities for the human serine/threonine kinome. Nature *613*, 759–
942 766.

943 60. Attwood, M.M., Fabbro, D., Sokolov, A.V., Knapp, S., and Schiöth, H.B. (2021). Trends in kinase
944 drug discovery: targets, indications and inhibitor design. Nat. Rev. Drug Discov. *20*, 839–861.

945 61. Eduati, F., Jaaks, P., Wappler, J., Cramer, T., Merten, C.A., Garnett, M.J., and Saez-Rodriguez, J.
946 (2020). Patient-specific logic models of signaling pathways from screenings on cancer biopsies to
947 prioritize personalized combination therapies. Mol. Syst. Biol. *16*, e8664.

948 62. Montagud, A., Béal, J., Tobalina, L., Traynard, P., Subramanian, V., Szalai, B., Alföldi, R., Puskás,
949 L., Valencia, A., Barillot, E., Saez-Rodriguez, J., and Calzone, L. (2022). Patient-specific Boolean
950 models of signalling networks guide personalised treatments. Elife *11*. 10.7554/eLife.72626.

951 63. Houstis, N., Rosen, E.D., and Lander, E.S. (2006). Reactive oxygen species have a causal role in
952 multiple forms of insulin resistance. Nature *440*, 944–948.

953 64. Fazakerley, D.J., Minard, A.Y., Krycer, J.R., Thomas, K.C., Stöckli, J., Harney, D.J., Burchfield,
954 J.G., Maghzal, G.J., Caldwell, S.T., Hartley, R.C., Stocker, R., Murphy, M.P., and James, D.E.
955 (2018). Mitochondrial oxidative stress causes insulin resistance without disrupting oxidative
956 phosphorylation. J. Biol. Chem. *293*, 7315–7328.

957 65. Su, Z., Burchfield, J.G., Yang, P., Humphrey, S.J., Yang, G., Francis, D., Yasmin, S., Shin, S.-Y.,
958 Norris, D.M., Kearney, A.L., Astore, M.A., Scavuzzo, J., Fisher-Wellman, K.H., Wang, Q.-P.,
959 Parker, B.L., Neely, G.G., Vafaee, F., Chiu, J., Yeo, R., Hogg, P.J., Fazakerley, D.J., Nguyen, L.K.,
960 Kuyucak, S., and James, D.E. (2019). Global redox proteome and phosphoproteome analysis
961 reveals redox switch in Akt. Nat. Commun. *10*, 5486.

962 66. Piazza, I., Kochanowski, K., Cappelletti, V., Fuhrer, T., Noor, E., Sauer, U., and Picotti, P. (2018).
963 A Map of Protein-Metabolite Interactions Reveals Principles of Chemical Communication. Cell
964 *172*, 358-372.e23.

965 67. Hicks, K.G., Cluntun, A.A., Schubert, H.L., Hackett, S.R., Berg, J.A., Leonard, P.G., Ajalla Aleixo,
966 M.A., Zhou, Y., Bott, A.J., Salvatore, S.R., Chang, F., Blevins, A., Barta, P., Tilley, S., Leifer, A.,
967 Guzman, A., Arok, A., Fogarty, S., Winter, J.M., Ahn, H.-C., Allen, K.N., Block, S., Cardoso, I.A.,
968 Ding, J., Dreveny, I., Gasper, W.C., Ho, Q., Matsuura, A., Palladino, M.J., Prajapati, S., Sun, P.,
969 Tittmann, K., Tolan, D.R., Unterlass, J., VanDemark, A.P., Vander Heiden, M.G., Webb, B.A.,
970 Yun, C.-H., Zhao, P., Wang, B., Schopfer, F.J., Hill, C.P., Nonato, M.C., Muller, F.L., Cox, J.E.,
971 and Rutter, J. (2023). Protein-metabolite interactomics of carbohydrate metabolism reveal
972 regulation of lactate dehydrogenase. Science *379*, 996–1003.

973 68. Sano, H., Kane, S., Sano, E., Mîinea, C.P., Asara, J.M., Lane, W.S., Garner, C.W., and Lienhard,
974 G.E. (2003). Insulin-stimulated phosphorylation of a Rab GTPase-activating protein regulates
975 GLUT4 translocation. J. Biol. Chem. *278*, 14599–14602.

976 69. Yardeni, T., Eckhaus, M., Morris, H.D., Huizing, M., and Hoogstraten-Miller, S. (2011). Retro-
977 orbital injections in mice. Lab Anim. *40*, 155–160.

978 70. Goodner, C.J., Hom, F.G., and Berrie, M.A. (1980). Investigation of the effect of insulin upon
979 regional brain glucose metabolism in the rat in vivo. Endocrinology *107*, 1827–1832.

980 71. Storey, J.D. (2002). A direct approach to false discovery rates. J. R. Stat. Soc. Series B Stat.
981 Methodol. *64*, 479–498.

982 72. Carlson, M. (2019). org. Mm. eg. db: Genome wide annotation for Mouse. R package version 3.2.
983 3. Bioconductor. London, United Kingdom: Genome Biology (BMC).

984 73. Carey, A.L., Steinberg, G.R., Macaulay, S.L., Thomas, W.G., Holmes, A.G., Ramm, G., Prelovsek,
985 O., Hohnen-Behrens, C., Watt, M.J., James, D.E., Kemp, B.E., Pedersen, B.K., and Febbraio, M.A.
986 (2006). Interleukin-6 increases insulin-stimulated glucose disposal in humans and glucose uptake
987 and fatty acid oxidation in vitro via AMP-activated protein kinase. Diabetes *55*, 2688–2697.

988 74. Krycer, J.R., Elkington, S.D., Diaz-Vegas, A., Cooke, K.C., Burchfield, J.G., Fisher-Wellman,
989 K.H., Cooney, G.J., Fazakerley, D.J., and James, D.E. (2020). Mitochondrial oxidants, but not
990 respiration, are sensitive to glucose in adipocytes. J. Biol. Chem. *295*, 99–110.

991 75. Masson, S.W.C., Woodhead, J.S.T., D'Souza, R.F., Broome, S.C., MacRae, C., Cho, H.C., Atiola,
992 R.D., Futi, T., Dent, J.R., Shepherd, P.R., and Merry, T.L. (2021). β-Catenin is required for optimal
993 exercise- and contraction-stimulated skeletal muscle glucose uptake. J. Physiol. *599*, 3897–3912.

994

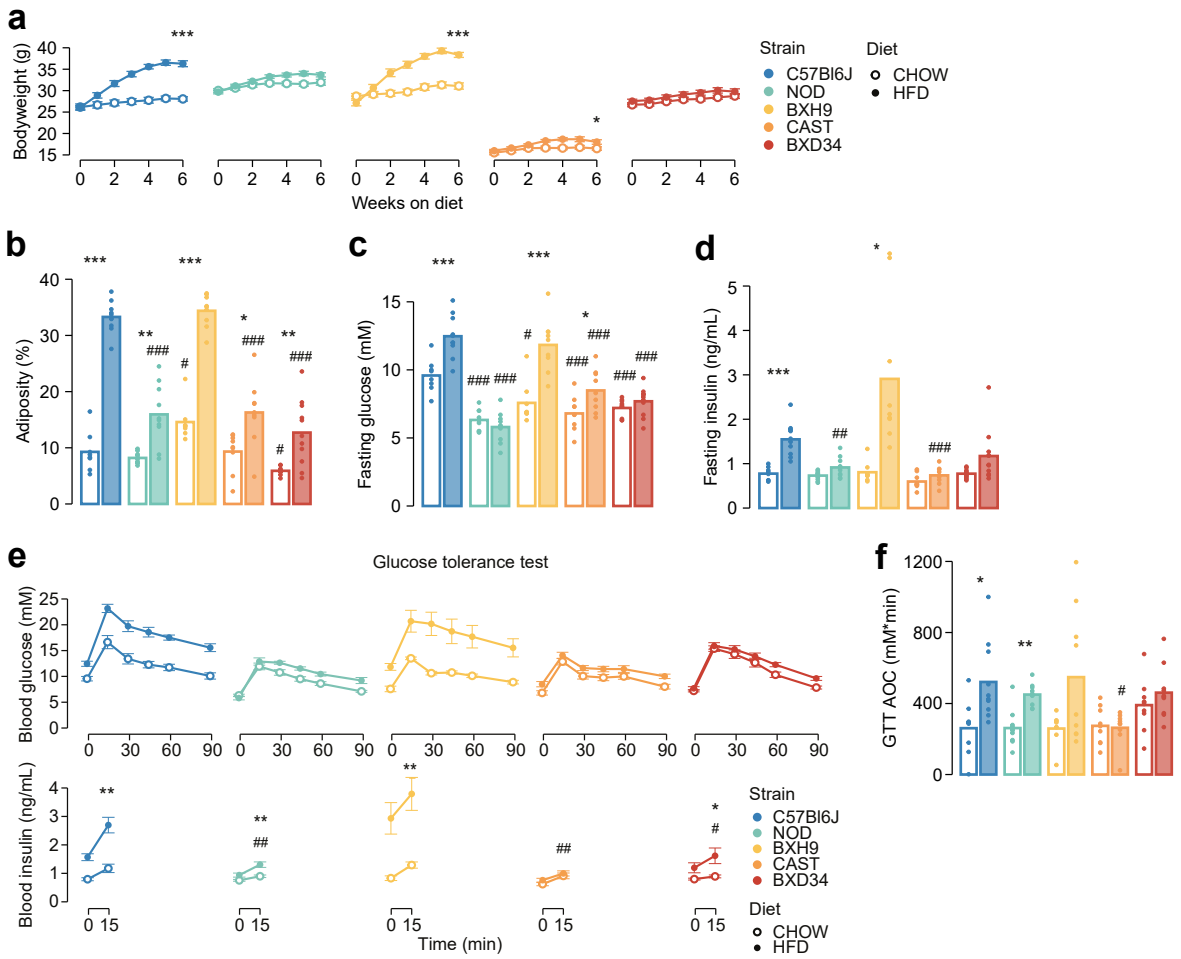

Figure S1: Genetics and diet alter morphometric and metabolic phenotypes. Related to Fig. 1. **a)** Mouse bodyweight was measured during a six-week diet regimen. Two-sided t-tests were performed to compare HFD to CHOW within each strain after six weeks, following Benjamini-Hochberg p-value adjustment (*). **b-d)** Measurement of **b)** adiposity, **c)** fasting blood glucose, and **d)** fasting blood insulin at the end of the diet regimen. **e)** At the end of the diet regimen a glucose tolerance test was performed. **f)** The area of the blood glucose curve (GTT AOC) was calculated. In **b-e)**, two-sided t-tests were performed to compare HFD to CHOW within each strain (*) or to compare each strain to C57Bl6J within either diet (#). P-values were adjusted by the Benjamini-Hochberg procedure. Error bars indicate SEM. In **e)** t-tests were only performed on 15-minute blood insulin levels. No comparisons across strains on CHOW were significant. n = 8-11 biological replicates. */#: $0.01 \leq p < 0.05$, **/##: $0.001 \leq p < 0.01$, ***/###: $p < 0.001$

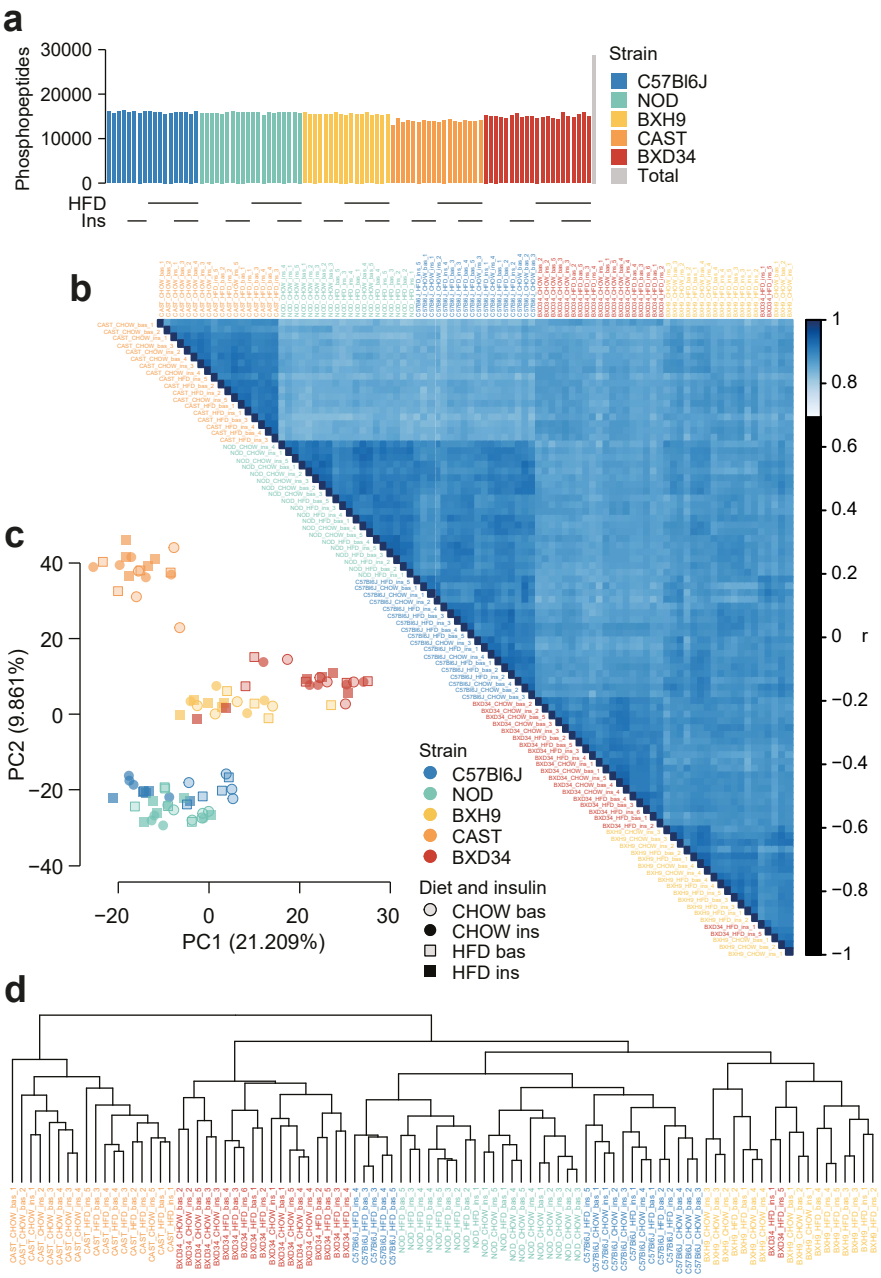

Figure S2: Quality control analysis of phosphoproteomics data. Related to Fig. 1. **a)** The number of unique class I phosphopeptides quantified in each sample and in total. **b)** Pearson's correlation was performed between each pair of samples. Samples are ordered by hierarchical clustering. **c)** Principal component analysis was performed on the phosphoproteome. The first two principal components (PC1 and PC2) are plotted for each sample and the percentage of overall variance explained by each principal component is indicated. "bas": unstimulated, "ins": insulin-stimulated. **d)** Hierarchical clustering was performed on all samples.

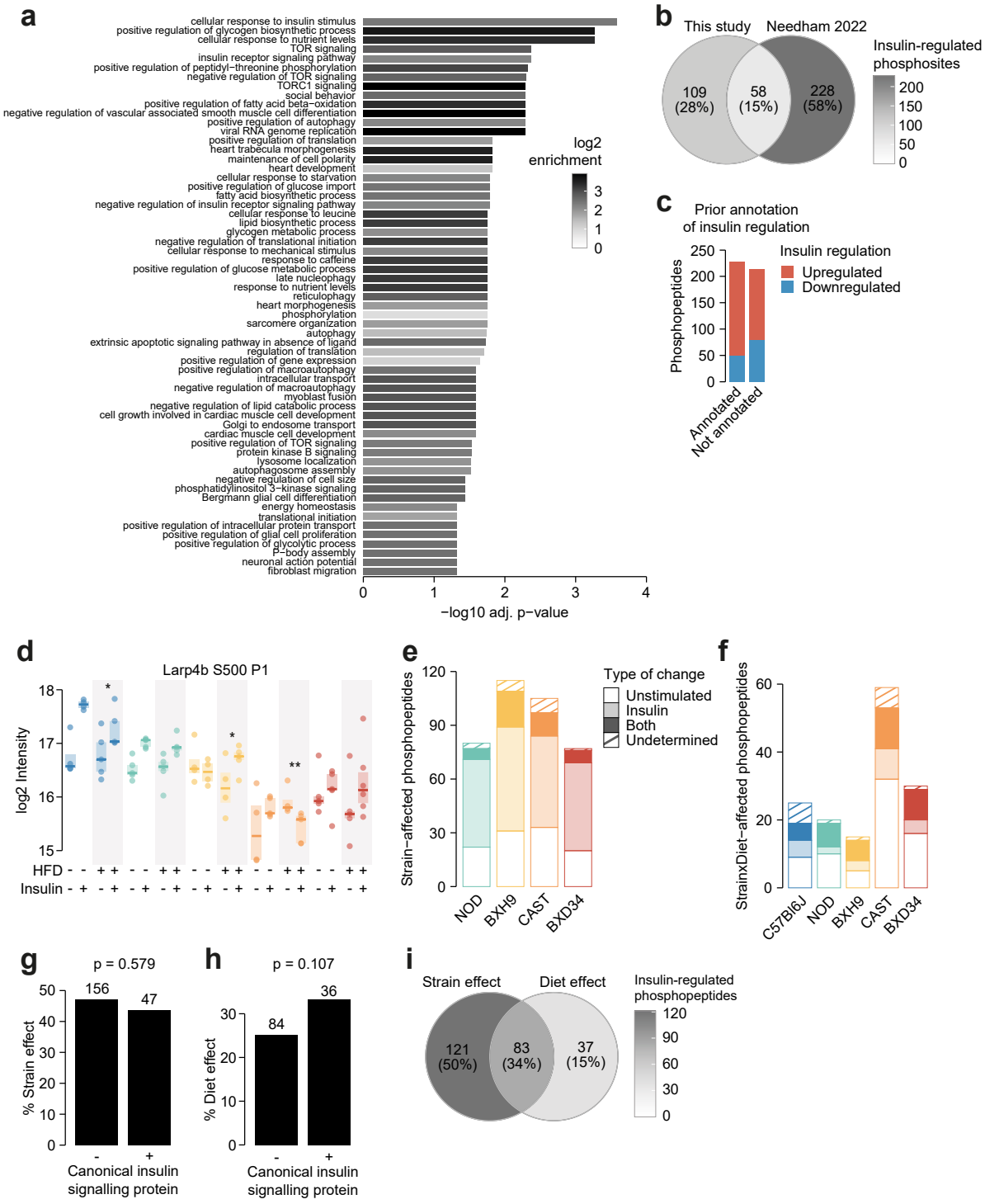

Figure S3: Characterisation of the insulin-regulated phosphoproteome. Related to Fig. 1-3. **a)** The enrichment of GO biological processes in genes containing insulin-regulated phosphopeptides relative to the entire phosphoproteome (one-sided Fisher's exact test, Benjamini-Hochberg p-value adjustment). Only significant pathways are shown (adj. $p < 0.05$). **b)** The number of phosphosites regulated by insulin in this study or a previous phosphoproteomic study of human skeletal muscle[1]. Only phosphosites quantified in both studies were considered. **c)** The number of insulin-regulated phosphopeptides with prior annotation of insulin regulation in the PhosphositePlus database[2]. **d)** A phosphopeptide where HFD-feeding enhanced insulin responses in BXH9 but suppressed insulin responses in C57Bl6J and CAST. A two-way ANOVA was

performed on insulin response values followed by two-sided t-tests comparing HFD to CHOW within each strain (q-values: *). **e)** Phosphopeptides with a Strain effect were examined to determine whether the effect was due to altered unstimulated phosphorylation ("Unstimulated"; Strain/C57Bl6J fold change > 1.3 in unstimulated samples), altered insulin-stimulated phosphorylation ("Insulin"; Strain/C57Bl6J fold change > 1.3 in insulin-stimulated samples), or both ("Both"). A proportion of phosphopeptides passed neither of these filters ("Undetermined"). **f)** The same analysis was performed on StrainxDiet-affected phosphopeptides, using the HFD/CHOW fold changes in either unstimulated or insulin-stimulated samples for each strain. **g-h)** The percentage of **g)** Strain effects and **h)** Diet effects (Uniform diet or StrainxDiet effect) among canonical or noncanonical insulin signalling proteins. P-values indicate two-sided Fisher's exact tests. The number of phosphopeptides in each group is shown. **i)** The overlap of Strain and Diet effects.

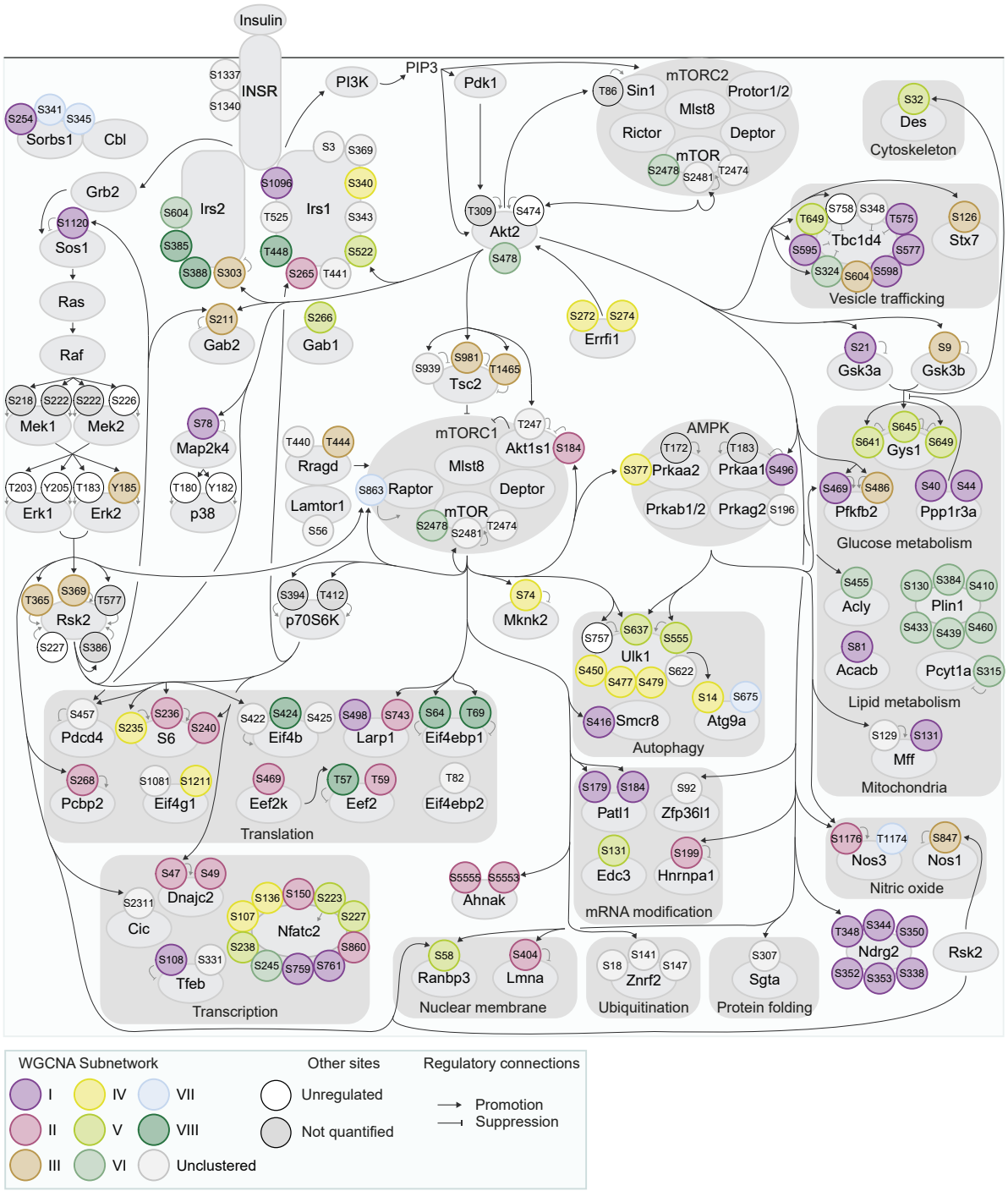

Figure S4: Organisation of insulin signalling subnetworks. Related to Fig. 5. The curated insulin signalling network displayed in Fig. 3 was annotated with WGCNA subnetworks from Fig. 5.

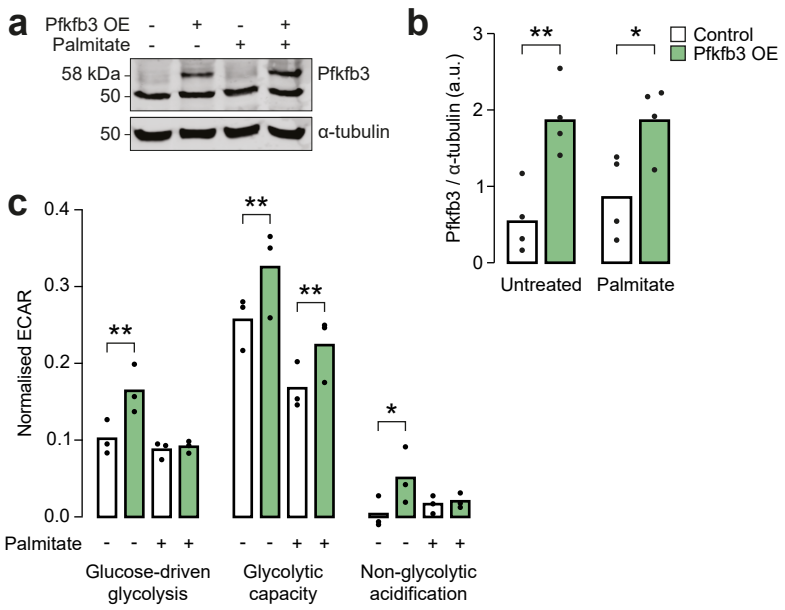

Figure S5: Overexpression of Pfkfb3 enhances glycolytic capacity. Related to Fig. 6. **a)** Representative blot and **b)** quantification for immunoblotting of Pfkfb3 in L6-GLUT4-HA myotubes with or without Pfkfb3 overexpression. Two-way ANOVA was performed followed by Šidák's post-hoc tests assessing the effect of Pfkfb3 overexpression (*). n = 4 biological replicates. **c)** Extracellular acidification rate (ECAR) in L6-GLUT4-HA myotubes treated with glucose (10 mM, "Glucose-driven glycolysis"), oligomycin (5 µg/mL, "Glycolytic capacity"), or 2-deoxyglucose (50mM, "Non-glycolytic acidification"). A two-way repeated measures ANOVA was performed followed by Tukey's posthoc tests comparing conditions within each of the three treatments (*). Not all significant comparisons are shown. n = 3 biological replicates. */#: $0.01 \leq p < 0.05$, **/##: $0.001 \leq p < 0.01$, ***/###: $p < 0.001$

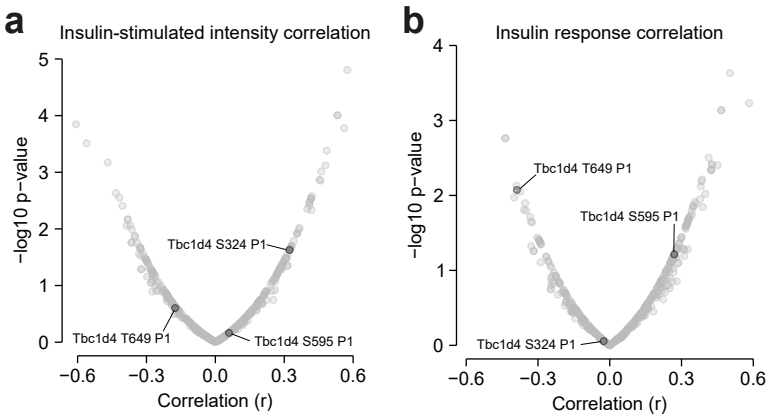

Figure S6: Correlation of Tbc1d4 regulatory sites with glucose uptake. Related to Discussion. **a-b)** The correlation of insulin-stimulated glucose uptake with insulin-regulated phosphopeptides using **a)** insulin-stimulated phosphopeptide intensity, or **b)** phosphopeptide insulin response values, as displayed in **Fig. 6**. Canonical regulatory phosphosites on Tbc1d4 are indicated. The fourth canonical regulatory site S758 was not analysed due to insufficient quantification (quantified in 4/94 samples).

Table S1: Muscle phosphoproteomics

(Page 1 "01_quantification") Normalized LFQ intensities of class I phosphopeptides. (Page 2 "02_analysis") Statistical analysis of phosphoproteome data.

Table S2: Insulin signalling subnetworks

WGCNA-derived subnetworks of insulin-regulated phosphopeptides.

Table S3: Association of kinase enrichment with insulin-stimulated glucose uptake

Pearson's correlation of KSEA enrichment scores with insulin-stimulated glucose uptake for all kinases with Strain or Diet effects. Correlation was performed on all values or on the medians of each Strain-Diet combination.

	Correlating all values		***Correlating Strain-Diet medians***	
Kinase	**r**	**p**	**r**	**p**
SGK	0.026282557	0.85773407	-0.114513813	0.752760165
Aur	0.181856398	0.221176679	0.446186208	0.196168185
p90RSK	0.042637179	0.771137201	0.392619919	0.261741297
aPKC	0.020857899	0.886881337	0.059269839	0.870801728
GSK3	-0.023496391	0.872683503	0.200939915	0.577765996
CDK5	0.092355979	0.527940053	0.136553891	0.706796386
P38	0.186315084	0.199914602	0.202333014	0.575075383
CDK1	0.134654975	0.356287427	0.245970422	0.493328434
CK2	0.062152944	0.671383691	-0.206449396	0.567152858

Supplementary references

1. Needham, E.J., Hingst, J.R., Parker, B.L., Morrison, K.R., Yang, G., Onslev, J., Kristensen, J.M., Højlund, K., Ling, N.X.Y., Oakhill, J.S., Richter, E.A., Kiens, B., Petersen, J., Pehmøller, C., James, D.E., Wojtaszewski, J.F.P., and Humphrey, S.J. (2021). Personalized phosphoproteomics identifies functional signaling. Nat. Biotechnol. 10.1038/s41587-021-01099-9.
2. Hornbeck, P.V., Zhang, B., Murray, B., Kornhauser, J.M., Latham, V., and Skrzypek, E. (2015). PhosphoSitePlus, 2014: mutations, PTMs and recalibrations. Nucleic Acids Res. *43*, D512-20.